Article

Cell Reports

An Essential Role for ECSIT in Mitochondrial Complex I Assembly and Mitophagy in Macrophages

Graphical Abstract

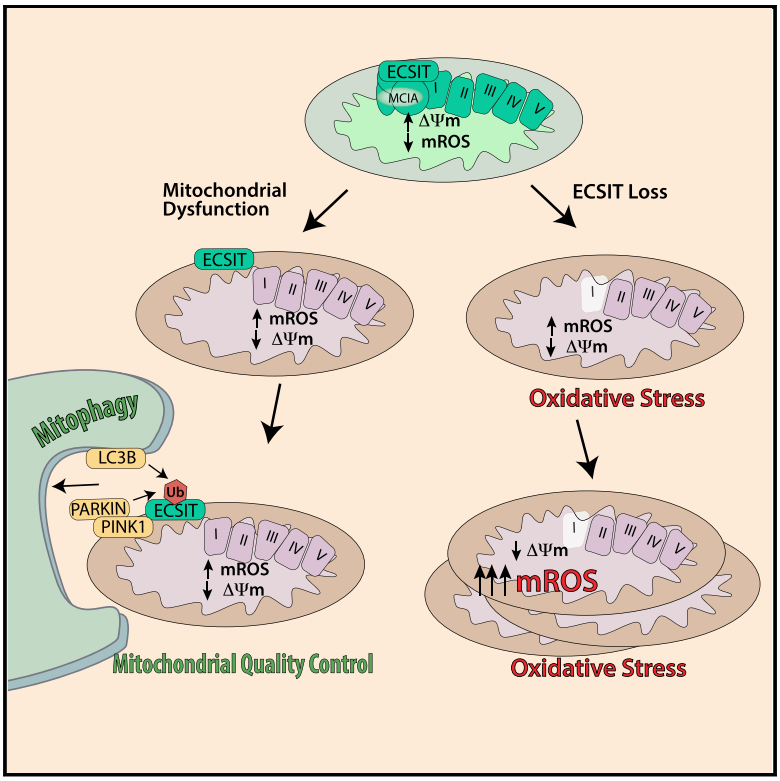

Highlights

- Loss of ECSIT in macrophages leads to a striking glycolytic shift
- ECSIT is essential for complex I assembly and stability in macrophages
- Role of ECSIT in mROS production and removal of damaged mitochondria by mitophagy

Authors

Flávia R.G. Carneiro, Alice Lepelley, John J. Seeley, Matthew S. Hayden, Sankar Ghosh

Correspondence

sg2715@columbia.edu

In Brief

Macrophages rely on fine-tuning their metabolism to fulfill their anti-bacterial functions. Carneiro et al. show that the complex I assembly factor ECSIT is an essential regulator of the balance between mitochondrial respiration and glycolysis and the maintenance of a healthy mitochondrial pool through mitophagy.

Carneiro et al., 2018, Cell Reports 22, 2654–2666
March 6, 2018
https://doi.org/10.1016/j.celrep.2018.02.051

CellPress

OPEN ACCESS
CellPress

Cell Reports
Article

An Essential Role for ECSIT in Mitochondrial Complex I Assembly and Mitophagy in Macrophages

Flávia R.G. Carneiro,[1,3,4] Alice Lepelley,[1,4] John J. Seeley,[1] Matthew S. Hayden,[1,2] and Sankar Ghosh[1,5,*]
[1]Department of Microbiology and Immunology, Vagelos College of Physicians and Surgeons, Columbia University, New York, NY 10032, USA
[2]Section of Dermatology, Department of Surgery, Dartmouth-Hitchcock Medical Center, Lebanon, NH 03756, USA
[3]FIOCRUZ, Center for Technological Development in Health (CDTS), Rio de Janeiro, Brazil
[4]These authors contributed equally
[5]Lead Contact
*Correspondence: sg2715@columbia.edu
https://doi.org/10.1016/j.celrep.2018.02.051

SUMMARY

ECSIT is a mitochondrial complex I (CI)-associated protein that has been shown to regulate the production of mitochondrial reactive oxygen species (mROS) following engagement of Toll-like receptors (TLRs). We have generated an *Ecsit* conditional knockout (CKO) mouse strain to study the *in vivo* role of ECSIT. ECSIT deletion results in profound alteration of macrophage metabolism, leading to a striking shift to reliance on glycolysis, complete disruption of CI activity, and loss of the CI holoenzyme and multiple subassemblies. An increase in constitutive mROS production in ECSIT-deleted macrophages prevents further TLR-induced mROS production. Surprisingly, ECSIT-deleted cells accumulate damaged mitochondria because of defective mitophagy. ECSIT associates with the mitophagy regulator PINK1 and exhibits Parkin-dependent ubiquitination. However, upon ECSIT deletion, we observed increased mitochondrial Parkin without the expected increase in mitophagy. Taken together, these results demonstrate a key role of ECSIT in CI function, mROS production, and mitophagy-dependent mitochondrial quality control.

INTRODUCTION

ECSIT (evolutionarily conserved signaling intermediate in Toll pathways) was originally identified as a highly conserved TRAF6-binding protein (Kopp et al., 1999; Xiao et al., 2003). Further studies showed that ECSIT is ubiquitinated by TRAF6 and has a role in intracellular bacterial clearance (West et al., 2011). ECSIT was shown to localize to mitochondria (Vogel et al., 2007) and regulate mitochondrial reactive oxygen species (mROS) production that occurs following engagement of Toll-like receptors (TLRs) (West et al., 2011). Phagocytosis of bacteria by macrophages results in ECSIT-dependent recruitment of mitochondria to the phagosomal membrane (Geng et al., 2015). There, ECSIT-dependent mROS production promotes activation of the phagosomal nicotinamide adenine dinucleotide phosphate (NADPH) oxidase system and ROS-dependent killing of engulfed microbes (West et al., 2011). ECSIT has also been described as a mitochondrial oxidative phosphorylation (OXPHOS) complex I (CI)-associated protein (Vogel et al., 2007). However, the link between ECSIT function as a CI accessory protein and innate immune signaling has remained unclear.

CI is the largest of the five OXPHOS complexes in the mitochondrial inner membrane. CI consists of 44 core and accessory subunits encoded in the mitochondrial and nuclear genomes. Its assembly is a highly complicated process that involves at least 14 additional assembly factors and stepwise assembly of intermediate subcomplexes (Guerrero-Castillo et al., 2017). CI and complex II (CII) are the entry points for electrons from NADH and FADH2, respectively. Electrons are then transferred to complex III (CIII) and complex IV, generating proton translocation from the mitochondrial matrix into the mitochondrial intermembrane space and establishing a proton motive force that drives generation of ATP through F_1F_0-ATP synthase (complex V) (reviewed by Sazanov, 2015).

The most commonly observed mitochondrial disorders are associated with CI dysfunction. Although CI disorders can result in variable and severe phenotypes, so far, few CI subunits have been targeted for deletion or knockdown in mice. Importantly, a number of CI deficiencies result from mutations in CI subunits critical for CI assembly (Alston et al., 2016; Bénit et al., 2003; Kirby et al., 1999; Koene et al., 2012; Loeffen et al., 2000; Mckenzie and Ryan, 2010; Nouws et al., 2010; Petruzzella and Papa, 2002). ECSIT interacts with the CI assembly factors NDUFAF1 and ACAD9 and was shown, using RNAi knockdown approaches, to be important for CI assembly and NDUFAF1 and ACAD9 stability in mitochondria in the HeLa and HEK293 cell lines (Nouws et al., 2010; Vogel et al., 2007). Furthermore, it was observed that CI levels were reduced, and a 500-kDa CI intermediate accumulated in ECSIT knockdown cells (Vogel et al., 2007). These results suggest that assembly or stability of the CI 1-MDa holoenzyme requires ECSIT. Importantly, although the levels of NDUFAF1 were severely impaired in these studies, the levels of NDUFS3 and ND1, two other CI subunits, remained unchanged (Vogel et al., 2007). Given the important role of NDUFAF1 and ACAD9 in CI assembly, it seemed that ECSIT

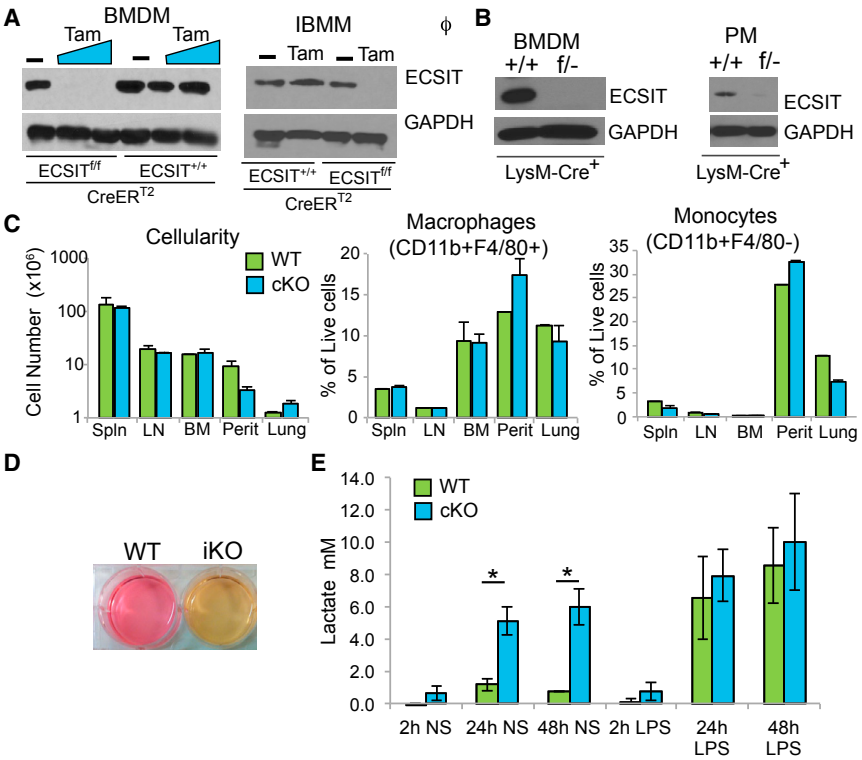

Figure 1. Conditional Deletion of ECSIT in Macrophages Leads to Metabolic Alterations

(A) Immunoblotting for ECSIT in lysates from ECSIT$^{+/+}$/Cre-ERT2^{+} and ECSIT$^{f/f}$/Cre-ERT2^{+} bone-marrow-derived macrophages (BMDMs) 7 days after deletion induction with tamoxifen (Tam) or vehicle (–) (left) and ECSIT$^{f/f}$/Cre-ERT2^{+} immortalized BMDMs (iBMMs) treated with vehicle (WT) or tamoxifen (iKO) for 48 hr and cultured for 5 days (right). For subsequent figures, IBMMs were assessed 5–12 days after induction of deletion.

(B) ECSIT levels in ECSIT$^{+/+}$/LysM-Cre^{+} (WT) and ECSIT$^{f/-}$/LysM-Cre^{+} (cKO) BMDMs and peritoneal macrophages (PMs).

(C) Cellularity and proportion in live cells of macrophages (CD11b+ F4/80+) and monocytes (CD11b+ F4/80–) from the spleen (Spln), lymph nodes (LNs), bone marrow (BM), peritoneal cavity (Perit), and lungs of WT and cKO mice (n = 3).

(D) Phenol red-containing cell culture media from ECSIT iKO and WT IBMMs.

(E) Lactate in supernatants from WT or cKO BMDMs, unstimulated (NS) or LPS-stimulated (100 ng/mL) (n = 2).

Shown are means ± SD of n experiments. *p < 0.05 in t test. See also Figure S1.

might predominantly function in concert with these CI assembly factors as part of a central CI assembly complex, the mitochondrial CI assembly (MCIA) (Guerrero-Castillo et al., 2017; Heide et al., 2012; Nouws et al., 2010; Vogel et al., 2007). The function of the MCIA complex is supported by the existence of CI deficiency in patients harboring mutations in genes encoding components of this complex (Alston et al., 2016; Fassone et al., 2011; Mimaki et al., 2012; Nouws et al., 2010). So far, only one ECSIT mutation has been identified in human disease, the V140A variant that triggers hyperinflammation and promotes hyperphagocytic syndrome in extranodal natural killer/T cell lymphoma (ENKTL) (Wen et al., 2018). Furthermore, ECSIT function has only been examined using downregulation in cell lines.

Interestingly, organization of the respiratory chain in macrophages, in particular adaptations in CI and complex II, has recently been shown to be instrumental for resistance to bacterial infection (Garaude et al., 2016; Kelly et al., 2015). Therefore, we decided to examine CI assembly and the expression of CI proteins upon ECSIT deletion in macrophages. Traditional *Ecsit* knockout (KO) mice have been generated; however, ECSIT deletion results in embryonic lethality, preventing the derivation of KO macrophages (Xiao et al., 2003). To overcome this difficulty, we have generated a conditionally targeted *Ecsit* knockout (CKO) mouse strain. Here we show that ECSIT can be efficiently deleted in macrophages derived from this mouse strain. ECSIT deletion leads to a metabolic shift in macrophages, accompanied by a complete loss of CI function and an increase in baseline mROS production. Strikingly, we also observed that, despite loss of mitochondrial membrane potential, ECSIT-deleted macrophages exhibit increased mitochondrial mass, suggesting a defect in the mitochondrial quality control pathway involving selective autophagy of damaged mitochondria, or mitophagy. Further analysis revealed that ECSIT interacts with several components of the PINK1/Parkin-dependent mitophagy pathway. Our studies therefore identify ECSIT as a crucial regulator of not only mitochondrial OXPHOS but also of inducible mROS production and mitophagy-dependent mitochondrial quality control.

RESULTS

Conditional Deletion of ECSIT in Macrophages

To study the role of ECSIT in mitochondria, and avoid the difficulties posed by early embryonic lethality of the traditional KO mice, we generated an *Ecsit* CKO mouse (Figure S1). Exon 3 in the *Ecsit* gene is shared among all three splice variants described in mice, and, therefore, deletion of exon 3 ensures the inactivation of all isoforms of *Ecsit* (Figure S1; Supplemental Experimental Procedures). Mice with the floxed (f) *Ecsit* allele were crossed either to Cre-ERT2 or LysM-Cre mice. Use of tamoxifen (Tam) resulted in complete deletion of *Ecsit* in cultured macrophages from ECSIT$^{f/f}$/Cre-ERT2^{+} mice compared with macrophages from ECSIT$^{+/+}$/Cre-ERT2^{+} mice (Figures 1A, left, and S1D), whereas generation of ECSIT$^{f/-}$/LysM-Cre^{+} mice (cKO), carrying one floxed allele and one traditional KO allele of ECSIT, resulted in efficient deletion of ECSIT in macrophages both *in vitro* (bone marrow-derived macrophages [BMDMs]) and *in vivo* (peritoneal macrophages [PMs]) (Figure 1B). Surprisingly, given the early embryonic lethality resulting from germline *Ecsit* deletion, deletion of ECSIT only in

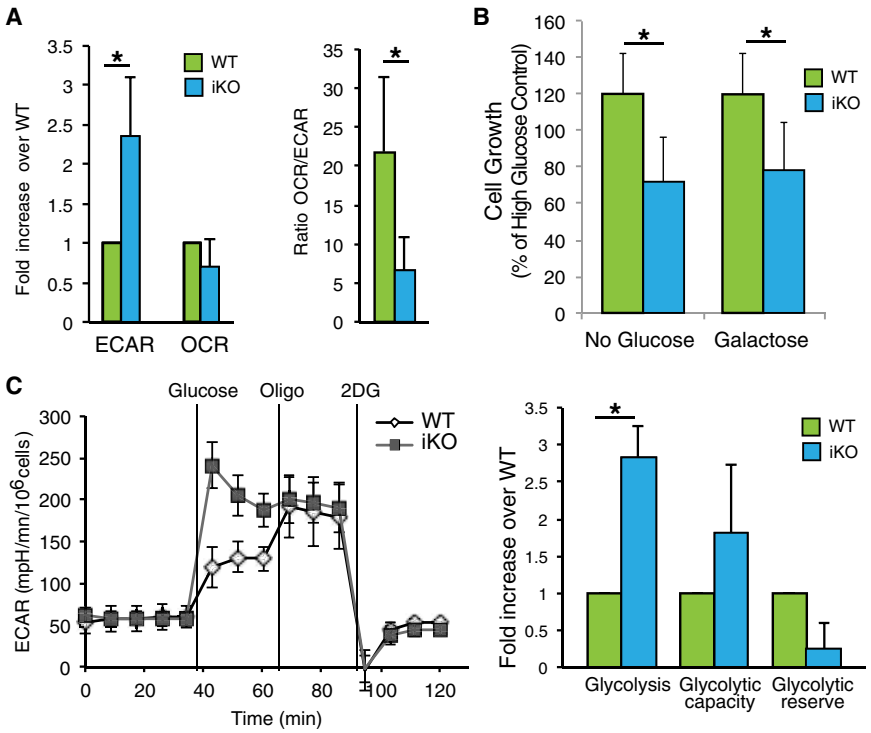

Figure 2. Increased Glycolysis in ECSIT-Deleted Macrophages

(A) Extracellular acidification rate (ECAR) and oxygen consumption rate (OCR) measured in WT and iKO cells (left) and OCR/ECAR ratio (right) (n = 3).

(B) Cell growth measured by crystal violet staining of IBMMs maintained for 48 hr in DMEM without glucose with or without galactose, 5 days after deletion induction (n = 5).

(C) The ECAR was assessed after addition of glucose, oligomycin (oligo), and 2-deoxyglucose (2DG). Left: time course of a representative experiment. Right: determination of glycolysis rate, glycolytic capacity, and glycolytic reserve (n = 2).

Means ± SD of n experiments are shown. *$p < 0.05$ in t test. See also Figures S2 and S3.

macrophages had no significant effect on macrophage or monocyte numbers in various tissues (Figure 1C). Therefore, we were able to proceed with the use of conditional ablation of ECSIT to study the role of ECSIT in macrophage metabolism and function. For convenience, we have designated ECSIT$^{f/-}$/LysM-Cre^{+} BMDMs as cKO macrophages. In addition, we immortalized BMDMs (IBMMs) from the ECSIT$^{f/f}$/Cre-ERT2^{+} mouse to use in future experiments. IBMMs were treated with 500 nM of tamoxifen (induced knockout [iKO]) or vehicle (wild-type [WT]) for 48 h and washed and cultured for 5–12 days prior to examining ECSIT levels by western blot (Figure 1A, right).

After ECSIT deletion, the iKO IBMM and cKO BMDM culture supernatants displayed a pronounced change of the phenol red pH indicator in the cell culture medium, suggesting that ECSIT-deleted cells were producing more acidic molecules than WT cells (Figure 1D and data not shown), which is reflective of a dramatic shift in metabolic activity. Genetic defects in CI can be accompanied by lactic acidosis resulting from a metabolic shift toward glycolysis (Bet et al., 1990; Houshmand et al., 1996). Consistent with this observation, there were higher levels of lactate in culture supernatants of cKO BMDMs (Figure 1E) and iKO IBMMs (data not shown), suggesting increased glycolytic activity in both BMDMs and IBMMs. Furthermore, although there was a significant increase in lactate production in lipopolysaccharide (LPS)-stimulated macrophages, consistent with the known glycolytic shift accompanying TLR stimulation (Kelly et al., 2015), there was no significant increase in lactate release in LPS-stimulated ECSIT cKO cells compared with unstimulated cKO cells (Figure 1E). Taken together, these results suggest a significant metabolic shift upon ECSIT deletion in macrophages.

ECSIT Deletion in Macrophages Leads to Changes in Cellular Energetics

To further investigate the metabolic effects of ECSIT deletion in macrophages, we used extracellular flux analysis to measure the extracellular acidification rate (ECAR), indicative of aerobic glycolysis, and oxygen consumption rate (OCR), indicative of mitochondrial respiration. ECSIT-deleted cells displayed a higher ECAR, consistent with increased lactate release and enhanced glycolysis (Figure 2A, left). Although the OCR was not significantly different between WT and iKO cells, there was a significant difference in the ratio between OCR and ECAR (OCR/ECAR), confirming the substantial metabolic shift seen upon ECSIT deletion (Figure 2A, right).

To better understand the macrophage adaptations resulting from ECSIT deletion, we followed cell survival and proliferation in restricted substrate conditions. As expected, ECSIT deletion impaired growth in medium without glucose (Figure 2B). Similar growth impairment was observed when ECSIT-deleted cells were cultured with galactose alone, which does not allow the net production of ATP from glycolysis (Figure 2B). To confirm the increased reliance of macrophages lacking ECSIT on glycolysis, we cultured macrophages in the presence of oxamate, an LDH inhibitor required for lactic acid release and completion of glycolysis. ECSIT iKO macrophages were more sensitive to oxamate than control macrophages (Figure S2A). Consistent with the importance of pyruvate metabolism for lactate production, ECSIT-deleted macrophages benefited more from pyruvate supplementation than WT macrophages (Figure S2B). Furthermore, iKO macrophages were more sensitive to replacement of glucose with glutamine, suggesting that glutamine metabolism and the tricarboxylic acid (TCA) cycle are impaired (Figure S2C).

Given the increase in lactate production and reliance on glucose for proliferation, we further characterized glycolysis in WT and ECSIT iKO macrophages by measuring the ECAR under different metabolic conditions: after addition of glucose

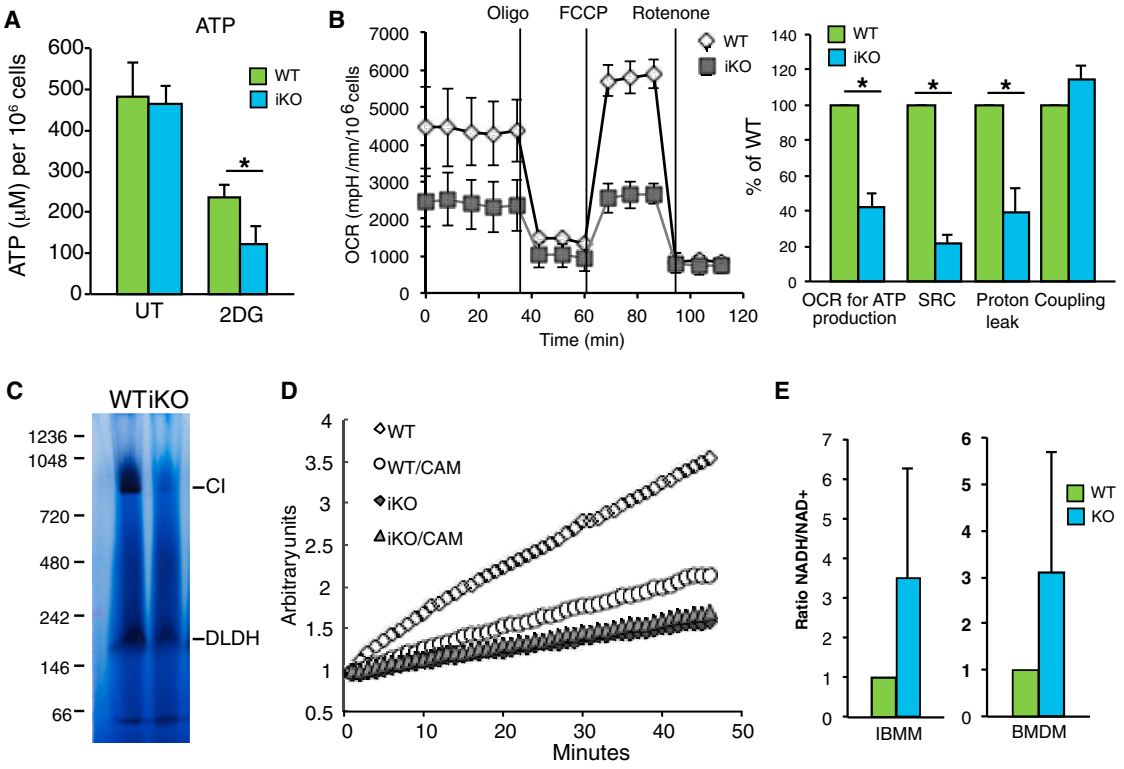

Figure 3. Loss of CI Activity in the Absence of ECSIT

(A) ATP levels in iKO and WT IBMMs left untreated (UT) or treated with 50 mM 2DG for 4 hr (n = 3).

(B) OCR in iKO and WT IBMMs, measured after addition of oligomycin, FCCP, and rotenone. Left: time course of a representative experiment. Right: determination of the OCR used for ATP production. SRC, spare respiratory capacity, OCR because of proton leak, and coupling efficiency (n = 2).

(C) CI in-gel activity of mitochondrial complexes from WT and iKO IBMMs; shown is a representative experiment (n = 3). DLDH, dihydrolipoamide dehydrogenase.

(D) CI activity in WT and iKO IBMM mitochondria; CAM, chloramphenicol; shown is a representative experiment (n = 3).

(E) NADH/NAD$^+$ ratio in lysates of iKO IBMMs (n = 2) and cKO BMDMs (n = 3) compared with WT cells.

Shown are means ± SD of n experiments. *$p < 0.05$ in t test.

to enable glycolysis; after addition of oligomycin (Oligo), which inhibits mitochondrial ATP synthase, thereby forcing glycolysis; and after addition of the glycolysis inhibitor 2-deoxyglucose (2DG) to confirm the specificity of glycolysis induction. Glycolysis was enhanced after addition of glucose in iKO IBMMs; however, glycolytic capacity (the maximum glycolysis rate in the presence of oligomycin) and glycolytic reserve (the quantitative difference between maximum glycolysis and basal glycolysis) were not significantly different from WT IBMMs (Figure 2C). These changes do not reflect a glycolytic reprogramming at the level of gene expression because mRNA levels of main glycolytic regulators and enzymes, including lactate dehydrogenase A (LDHA) and MCT1, were unchanged in iKO IBMMs (Figure S3). Taken together, these results suggest that CI impairment results in enhanced glycolytic flux in ECSIT-deleted IBMMs.

ECSIT Is Required for CI Function and Mitochondrial OXPHOS

Consistent with the increased reliance of ECSIT-deleted macrophages on glucose, we found that inhibition of glycolysis with 2DG resulted in a more profound decrease in ATP levels in ECSIT iKO and cKO macrophages compared with WT controls (Figure 3A and data not shown). Thus, ECSIT KO cells were more dependent on glycolysis for ATP production, suggesting that increased glycolysis might be a mechanism to compensate for the defect in mitochondrial respiration. We measured the OCR in WT and iKO IBMMs after sequential addition of oligomycin to abrogate the use of OXPHOS and oxygen for ATP production, the protonophore carbonyl cyanide-4-(trifluoromethoxy)phenylhydrazone (FCCP) to dissipate the proton gradient leading to oxygen reduction independent of ATP production, and finally the electron transport chain inhibitor rotenone to confirm the specificity of respiratory chain function and identify the level of OXPHOS-independent OCR. ECSIT-deleted IBMMs had a markedly decreased spare respiratory capacity (SRC), as defined by the quantitative difference between the maximal OCR induced by FCCP and the initial basal OCR (Figure 3B). IBMMs lacking ECSIT also exhibited a decreased OCR used for ATP production and proton leak (Figure 3B). Notably, each of these functions depends on establishment of the proton gradient across the mitochondrial inner membrane. This suggests that proton translocation and the mitochondrial membrane potential are impaired in ECSIT-deleted cells, consistent with CI dysfunction. In contrast, coupling (the amount of oxygen consumed to make ATP) was

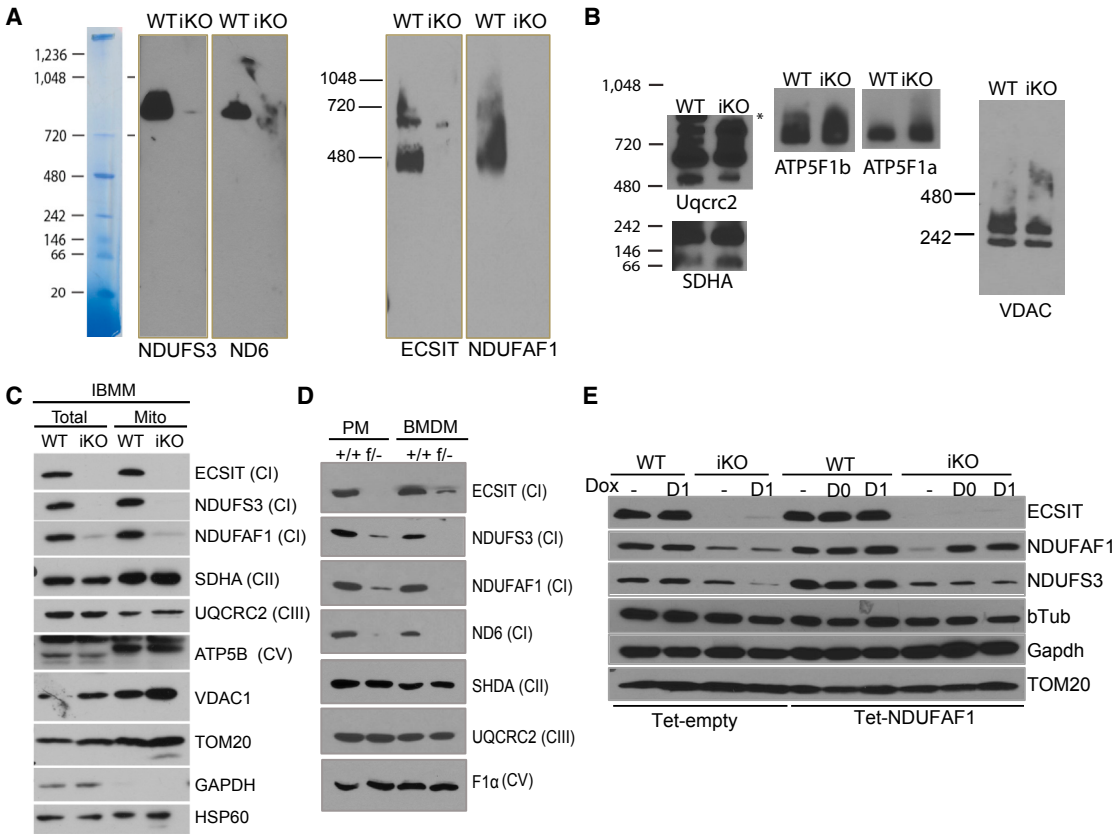

Figure 4. Loss of CI Proteins in ECSIT-Deleted Macrophages

(A and B) BN-PAGE followed by western blot of mitochondrial complexes from WT and iKO IBMMs detected with the indicated proteins from (A) complex I and (B) complexes II, III, V, and VDAC1.

(C and D) Immunoblot of OXPHOS proteins in (C) mitochondrial preparation and total cell lysates of IBMM and (D) total cell lysate of BMDM and PMs.

(E) Immunoblotting of IBMMs transduced with doxycycline-inducible NDUFAF1 (Tet-NDUFAF1) or control (Tet-Empty) and treated with tamoxifen on day 0 and day 1 to induce ECSIT deletion and doxycyclin (Dox) every 24 hr from day 0 or day 1 until analysis on day 3.

Shown are representative experiments (n = 3). See also Figure S4.

similar between WT and iKO cells, indicating that mitochondrial ATP synthase function is unaffected (Figure 3B, right). Thus, the residual OCR may come from CII function, but it cannot compensate for CI dysfunction in energy-demanding situations, assessed under maximal respiration conditions. Therefore, ECSIT-deleted macrophages are likely to be more sensitive to metabolic stress, as can occur in inflammatory sites where macrophages fulfill their functions.

To directly examine CI function in the absence of ECSIT, we prepared mitochondria from WT and iKO cells and performed blue native gel electrophoresis (BN-PAGE) followed by in-gel CI activity. A complete lack of CI activity was observed in macrophages lacking ECSIT at the level of the 1-MDa holoenzyme, and no subcomplex with residual CI activity was detected (Figure 3C). Next we measured oxidation of NADH to nicotinamide adenine dinucleotide (NAD^+) and observed that CI NADH dehydrogenase activity was fully abolished in mitochondria from ECSIT-deleted macrophages (Figure 3D). Consistent with this finding, the NADH/NAD^+ ratio was higher in ECSIT-deleted macrophages (Figure 3E). Taken together with the observed glycolytic shift, these results suggest a complete loss of CI activity and strong impairment of OXPHOS.

ECSIT Is Required for CI Assembly and Stability of CI Proteins

Previously it was observed that proteins in other CI subcomplexes, such as NDUFS3, were minimally affected by small interfering RNA (siRNA)-mediated ECSIT knockdown (Nouws et al., 2010; Vogel et al., 2007). This suggested that, although ECSIT was pivotal for the formation or stability of ECSIT-containing assembly subcomplexes, other CI holoenzyme intermediates were not dependent on ECSIT. Given the profound disruption of CI activity observed in ECSIT-deleted macrophages (Figure 3), we performed BN-PAGE followed by western blotting to examine CI and the ECSIT-containing assembly complexes. Consistent with previous reports, we found that the levels of NDUFAF1 in the ECSIT-associated subcomplexes (≈400 kDa and 700 kDa) in mitochondrial preparations were significantly decreased (Figure 4A), suggesting that function of the MCIA complex might be impaired (Baertling et al., 2017; Guerrero-Castillo et al., 2017).

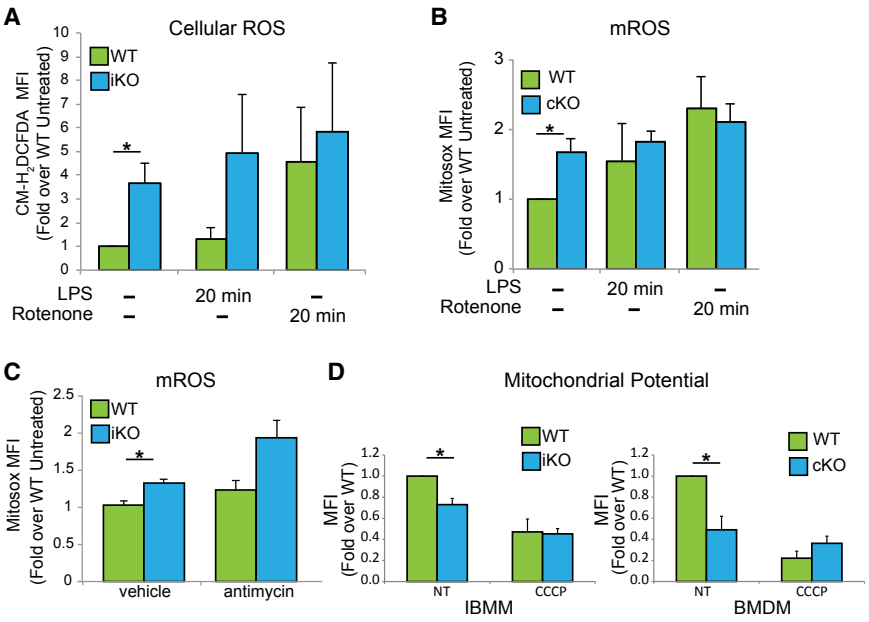

Figure 5. Mitochondrial Dysfunction in Cells Lacking ECSIT

(A) IBMMs stimulated with rotenone (1 μM) and LPS (100 ng/mL) for 20 min 7 days after deletion induction, stained with chloromethyl derivative of H2DCFDA (2',7'-dichlorodihydrofluorescein diacetate) (CM-H_2DCFDA) and analyzed by flow cytometry for total ROS (n = 3).

(B) BMDMs stimulated with rotenone and LPS for 20 min, stained with MitoSOX, and analyzed by flow cytometry for mROS (n = 3).

(C) IBMMs stimulated with antimycin A (5 μM) for 20 min and analyzed for mROS like in (B) (n = 3).

(D) $\Delta\psi_m$ measured by flow cytometry using tetramethylrhodamine, methyl ester (TMRM) in IBMMs and BMDMs, in the absence (non treated, NT) or presence of CCCP for 1 h (30 μM) (n = 3).

Shown are means ± SD of n experiments. *p < 0.05 in t test. See also Figure S5.

However, in contrast to previous reports, we found that other components of CI, NDUFS3 and ND6, were substantially diminished in ECSIT KO cells and importantly, did not accumulate in detectable assembly intermediates (Figure 4A). CII (succinate dehydrogenase complex, subunit A [SDHA]), complex III (Uqcrc2), and complex V (ATP5F1a and b) were unaffected (Figure 4B). Thus, ECSIT deletion in macrophages resulted in significant disruption of the CI holoenzyme and abrogation of CI subassembly formation without affecting other complexes of the respiratory chain.

To assess whether these results reflect a complete loss of CI proteins versus a failure of mitochondrial import, we performed immunoblotting for several CI components using mitochondrial and total cellular lysates from multiple macrophage types. Upon deletion of ECSIT, we observed a severe reduction in the assembly factor NDUFAF1 and ND6, not only in mitochondrial lysates of IBMMs but also in total cell lysates of IBMMs (Figure 4C), BMDMs, and PMs (Figure 4D). This suggests that ECSIT is essential for maintenance and/or stability of the early 293- and 357-kDa subcomplexes formed by ECSIT and ECSIT binding partners, NDUFAF1, ACAD9, and TMEM126B, components of the MCIA complex, and subsequent subcomplex intermediates, incorporating ND6 (Guerrero-Castillo et al., 2017). We also observed significant loss of another CI subunit, NDUFS3, which has been reported to assemble in an early 170-kDa subcomplex before intervention of ECSIT and the MCIA complex, suggesting broad effects of ECSIT deletion on assembly and abundance of CI subunits.

Given the role of ECSIT in the regulation of multiple transcription factor pathways (Kopp et al., 1999; Xiao et al., 2003), we assessed whether the changes in mitochondrial CI protein levels could be attributable to changes in gene expression. However, despite significant decreases in protein levels, mRNAs encoding these and other mitochondrial respiratory chain components were unchanged in ECSIT-deleted cells (Figure S4A). This suggested that the protein levels of CI subunits were regulated by post-translational mechanisms upon ECSIT loss. Inhibition of proteasomal or lysosomal protein degradation using MG132 or Bafilomycin A1 (BafA1), respectively, did not restore the protein levels of NDUFS3 and NDUFAF1 (Figure S4B), suggesting that other mitochondrial proteases (e.g., LON-ClpP; Pryde et al., 2016), might be responsible for degradation of CI subunits. To test whether the other main assembly factor, NDUFAF1, could rescue CI subunit levels, we reintroduced NDUFAF1 in ECSIT-deleted macrophages. IBMMs were stably transduced with a doxycycline-inducible lentivirus vector expressing NDUFAF1 (Tet-NDUFAF1) or an empty vector (Tet-empty). Cells were treated with tamoxifen to delete ECSIT and with doxycycline to induce NDUFAF1 expression at the same time (day 0), or 24 hr later (day 1). We observed that reintroduction of NDUFAF1 did not restore the protein level of NDUFS3 (Figure 4E), suggesting that the contribution of ECSIT to CI assembly is not simply to stabilize NDUFAF1. Taken together, these results demonstrate broad effects of ECSIT deletion on the composition of CI and a requirement for ECSIT in the maintenance or stability of both the CI holoenzyme and multiple CI subcomplexes.

Dysregulation of mROS Production and Loss of Mitochondrial Membrane Potential in Macrophages Lacking ECSIT

OXPHOS dysfunction is known to lead to ROS production (Brewer et al., 2013; Lin and Beal, 2006). Therefore, we examined the production of cellular ROS in WT and ECSIT-deleted macrophages. We observed a significant increase in total cellular ROS in ECSIT-deleted cells (Figure 5A). We previously showed that ECSIT was required for increased mROS production upon exposure of macrophages to bacterial pathogens and that ECSIT knockdown impaired this inducible mROS production without altering baseline levels (West et al., 2011). However, we found that the basal level of mROS was significantly

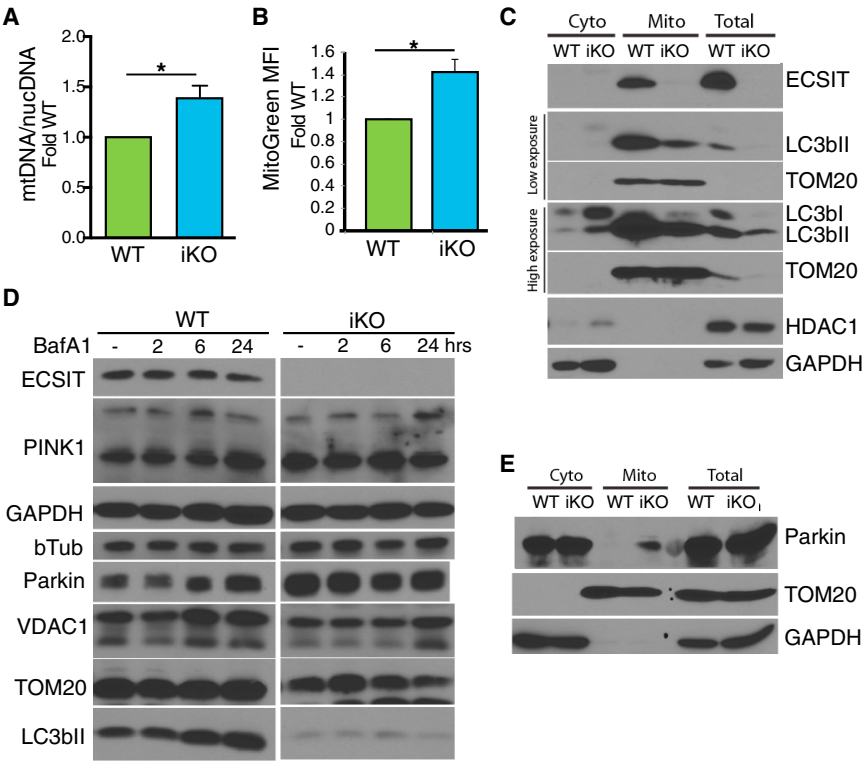

Figure 6. Altered Mitophagy in ECSIT-Deleted Macrophages

(A) Ratio of mitochondrial DNA (mtDNA) over nuclear DNA (nucDNA) copies, determined by qPCR in IBMMs 7 days after deletion induction (n = 4).

(B) IBMMs stained with mitotracker green and analyzed by flow cytometry (n = 4). (A and B) Fold change over WT. Shown are means ± SEM of n experiments. *p < 0.05 in t test.

(C and E) Western blot analysis of (C) LC3b and (E) Parkin in total lysate, isolated mitochondria, and cytosol of WT and iKO IBMM (representative experiment of n = 3).

(D) Western blot analysis of cellular lysates of WT and iKO IBMMs treated with 5 nM BafA1 (representative experiment of n = 3).

enhanced in ECSIT cKO BMDMs (Figure 5B), a finding consistent with oxidative stress stemming from CI dysfunction (Leadsham et al., 2013; Pagano et al., 2014; Pitkanen and Robinson, 1996). No further increase in ROS or mROS production was observed when ECSIT-deleted macrophages were treated with the CI inhibitor rotenone or LPS (Figures 5A and 5B). When macrophages were treated with antimycin to inhibit CIII, which, along with CI, is an important source of mROS production, we observed an increase in mROS in both WT and ECSIT-deleted macrophages (Figure 5C). Thus, although ECSIT-deficient cells retain the capacity to increase mROS production, they fail to do so upon LPS stimulation. This is not likely to be due to defects in the TLR signaling pathway because ECSIT-deleted BMDMs exhibit normal induction of the pro-inflammatory cytokines tumor necrosis factor alpha (TNF-α) and interleukin-6 (IL-6) following LPS exposure (Figure S5). These results are consistent with our previous finding that TLR-induced mROS production is dependent on ECSIT (West et al., 2011) and suggest that ECSIT may regulate mROS production during the innate immune response by regulating CI assembly and function.

Both direct analysis of CI and changes seen in macrophage metabolism suggest complete loss of CI function upon ECSIT deletion. Maintenance of mitochondrial membrane potential ($\Delta\psi_m$) is essential for mitochondrial function. Analysis of $\Delta\psi_m$, with uncoupler carbonyl cyanide m-chlorophenyl hydrazine (CCCP) treatment providing a control for collapsed mitochondrial $\Delta\psi_m$, revealed that ECSIT-deleted IBMMs and BMDMs have a lower $\Delta\psi_m$ compared with WT cells (Figure 5D). Thus, consistent with its role in CI assembly and function, loss of ECSIT results in the appearance of indicators of mitochondrial damage, including increased constitutive mROS production and decreased $\Delta\psi_m$. These defects also result in loss of LPS-inducible mROS production, which is critical for macrophage bactericidal function.

Defective Mitochondrial Quality Control in ECSIT-Deleted Macrophages

The loss of $\Delta\psi_m$ in macrophages lacking ECSIT should activate mitochondrial quality control through mitophagy, as occurs upon chemically induced mitochondrial damage (Ashrafi and Schwarz, 2013; Narendra et al., 2008). Therefore, we examined mitochondrial content in WT and ECSIT-deleted macrophages. Surprisingly, and despite decreased $\Delta\psi_m$ and increased mROS, we found increased mitochondrial DNA content in macrophages lacking ECSIT (Figure 6A). Similarly, we observed increased mitochondrial mass using mitotracker green, which stains mitochondria independently of $\Delta\psi_m$ (Figure 6B). To assess whether mitophagy is being triggered in ECSIT-deleted cells, we examined mitochondrial recruitment of LC3bII, a late-stage mitophagy marker necessary for lysosomal degradation. We observed a decrease in total and mitochondrial LC3bII protein levels in macrophages lacking ECSIT (Figure 6C). Loss of total LC3bII could indicate an increase in mitophagy or autophagic flux. However, when macrophages were treated with BafA1 to inhibit autophagy, we observed accumulation of LC3bII in WT but not ECSIT-deleted macrophages (Figure 6D). Likewise, the decreased accumulation of VDAC1, TOM20, and Parkin in ECSIT-deleted cells further confirmed that mitophagy was impaired (Figure 6D). These results suggest a role for ECSIT in selective autophagy of damaged mitochondria.

Upon loss of $\Delta\psi_m$, mitophagy is triggered through the PINK1/Parkin system. PINK1 is a ser/thr kinase that is normally imported to the inner mitochondrial membrane and constitutively degraded (Ashrafi and Schwarz, 2013). Upon loss of $\Delta\psi_m$, PINK1 import and, therefore, degradation are impaired, and PINK1 accumulates on the outer mitochondrial membrane (OMM) (Narendra et al., 2010). This results in Parkin recruitment and Parkin-dependent ubiquitination of target proteins on the

OMM. The ubiquitinated substrates are recognized by adaptor proteins, which mediate recruitment of LC3bII. Therefore, one reason for decreased LC3bII recruitment could be decreased Parkin levels at mitochondria. Instead, when mitochondrial Parkin was examined by western blot, both total and, especially, mitochondrial Parkin protein levels were increased in ECSIT-deficient cells (Figures 6D and 6E). This suggests that the mitochondrial damage that occurs following ECSIT deletion initiates PINK1/Parkin-dependent mitophagy but that Parkin accumulation fails to lead to LC3bII recruitment in the absence of ECSIT. Therefore, selective mitochondrial autophagy is impaired downstream of mitochondrial Parkin accumulation but upstream of LC3bII recruitment.

ECSIT Is a Parkin Substrate

To understand how ECSIT contributes to mitophagy, we investigated the interaction of ECSIT with components of the PINK1/Parkin mitophagy pathway. When co-expressed in 293FT cells, we observed co-immunoprecipitation of ECSIT with PINK1 (Figures 7A and 7B) (Beilina et al., 2005). This interaction was dependent upon mitochondrial localization of ECSIT because it was decreased with a mutant form of ECSIT lacking the mitochondrial localization sequence (Figure 7B; ΔMLS). Furthermore, we observed co-immunoprecipitation of ECSIT with LC3b upon induction of mitophagy with the uncoupling agent CCCP (Figure 7C). When we assessed ECSIT by immunoblotting following induction of mitochondrial damage by CCCP treatment of macrophages, we observed the rapid appearance of a slower-migrating form of ECSIT (Figure 7D, indicated by an arrow), consistent with post-translational modification, such as ubiquitination or stabilization, of full-length ECSIT containing the mitochondrial targeting sequence at the OMM. Interestingly, when immunoprecipitating PINK1, we only recovered the slower-migrating form of ECSIT, whereas the processed form of ECSIT, which co-migrates with ECSITΔMLS, did not interact with PINK1 (Figure 7B). Similarly, we observed interaction between endogenous ECSIT and full-length PINK1 at steady state in BMDMs and IBMMs. This was enhanced by treatment with BafA1 and CCCP, blocking degradation and inducing damage (Figures 7E and 7F). ECSIT also interacted with LC3bII upon mitochondrial damage induction. Furthermore, upon induction of mitochondrial damage and inhibition of autophagy with BafA1, we were able to observe accumulation of multiple slower-migrating forms of ECSIT (Figure 7G). Interestingly, we did not see accumulation of these higher-molecular-weight ECSIT species in the absence of BafA1 treatment (data not shown), suggesting that these species may be normally degraded by autophagic mechanisms. We have previously reported that LPS stimulation leads to accumulation of ECSIT at the OMM (West et al., 2011). Here we see that mitochondrial damage results in accumulation of unprocessed ECSIT (Figures 7C and 7D), ECSIT modification, and association with LC3b.

Given that ECSIT interacts with PINK1 and, upon mitochondrial damage, is likely ubiquitinated and associates with LC3b, we wondered whether ECSIT might be a substrate for Parkin. We therefore tested whether overexpression of Parkin, with or without PINK1, could induce ECSIT ubiquitination (Yoshii et al., 2011). When Parkin was expressed together with vesicular stomatitis virus (VSV)-tagged ubiquitin in 293FT cells, we observed increased ubiquitination of ECSIT (Figure 7H). Parkin-induced ECSIT ubiquitination was further increased by PINK1 co-expression (Figure 7H), consistent with the role of PINK1 in the mitochondrial recruitment of Parkin and activation of Parkin ubiquitin ligase activity. Furthermore, Parkin/PINK1-induced ECSIT ubiquitination was dependent on mitochondrial localization of ECSIT because it was not observed using ECSITΔMLS (Figure 7H). Taken together, these findings suggest that ECSIT may be an important substrate for PINK1/Parkin-mediated autophagy. Consequently, upon loss of ECSIT, both mitochondrial OXPHOS and mitochondrial quality control are impaired, resulting in accumulation of damaged mitochondria with increased mROS production.

DISCUSSION

We have successfully generated a conditional KO mouse for ECSIT, a mitochondrial CI assembly factor. The conditional KO mouse represents a unique model to study the function of ECSIT in different tissues and cell types. Macrophages lacking ECSIT exhibit profound disruption of mitochondrial CI. ECSIT deletion led to increased dependence on glycolysis and mitochondrial respiratory chain dysfunction. Although the observed increase in mROS production and decrease in $\Delta\psi_m$ would be expected to increase mitophagy, we observed an increase in mitochondrial mass. Activation and recruitment of the mitophagy machinery is disrupted in cells lacking ECSIT. We found that ECSIT undergoes ubiquitination following mitochondrial damage and that ECSIT can interact with PINK1, Parkin, and LC3bII. Finally, we showed that Parkin induces ubiquitination of mitochondrial ECSIT. Upon loss of ECSIT, we observed increased mitochondrial accumulation of Parkin, suggesting initiation of mitophagic pathways. However, LC3bII recruitment is diminished and accumulation of damaged mitochondria occurs. These results suggest that ECSIT is a key mediator of PINK1/Parkin-dependent mitophagy, allowing recruitment of the degradative autophagy machinery downstream of mitochondrial damage signaling. In the future, it will be important to determine which of the selective autophagy receptors mediate ECSIT-dependent LC3bII recruitment to damaged mitochondria or whether ECSIT can act as a mitophagy receptor to more fully elucidate the role of ECSIT in mitophagy.

ECSIT has previously been described as a CI chaperone and was identified in a subcomplex of 370 kDa known as the MCIA complex, containing TMEM126B, NDUFAF1, and ACAD9 (Heide et al., 2012). More recently, it has been reported that TMEM126B and another transmembrane protein, TIMMDC1, have a role in putting together two membrane arm subcomplexes (Andrews et al., 2013; Guarani et al., 2014). TIMMDC1 immunoprecipitated with ECSIT and NDUFAF1, and immunoprecipitation (IP)-mass spectrometry (MS) analysis showed several interactions of this protein with CI subunits, including all proteins of the MCIA complex (Guarani et al., 2014). The MCIA complex likely helps to assemble the membrane arm of CI with TIMMDC1 (Guerrero-Castillo et al., 2017). Previously, Vogel et al. (2007) showed that ECSIT knockdown reduced NDUFAF1 levels and impaired CI enzymatic activity and assembly in HeLa cells. Although the

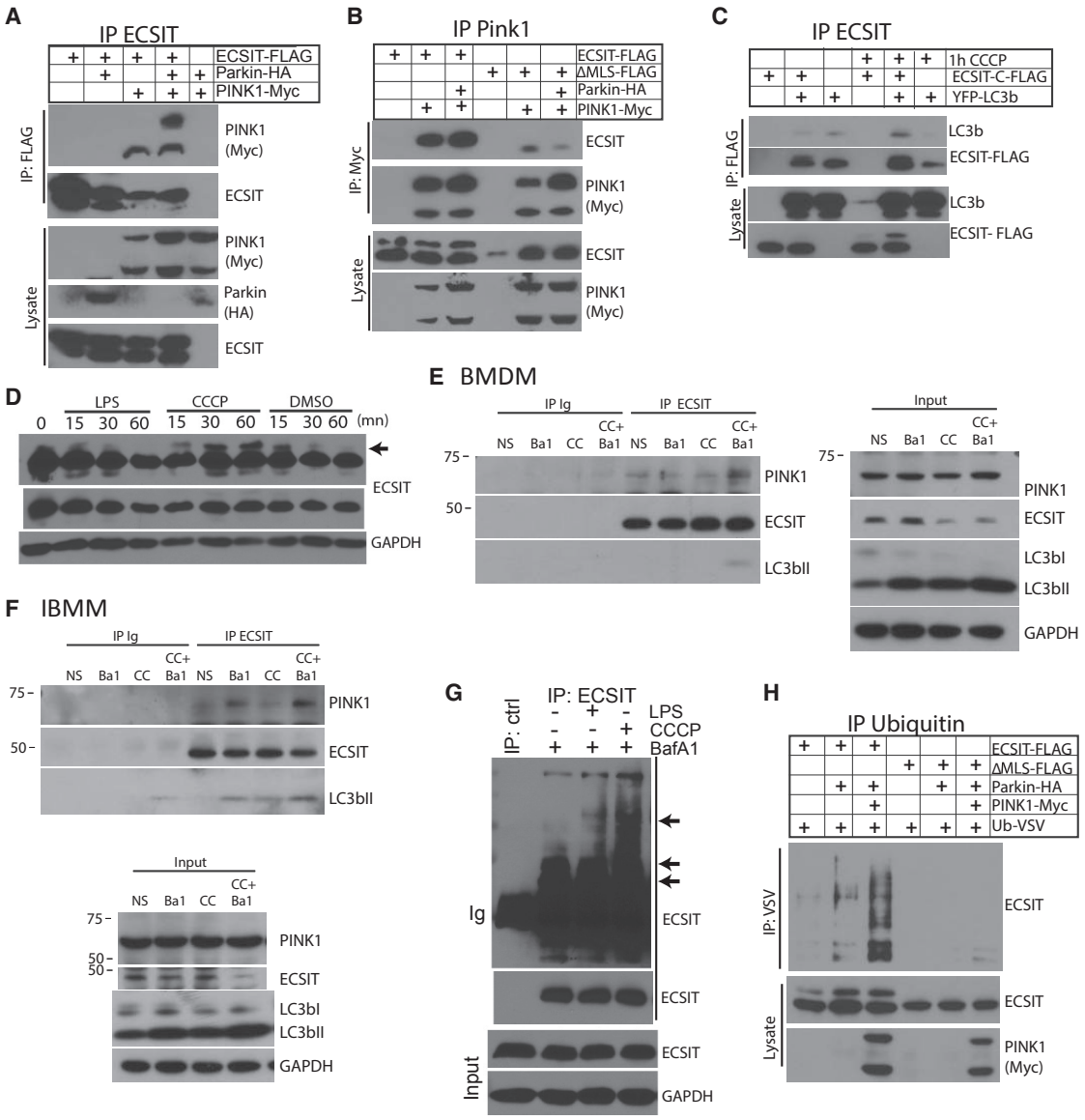

Figure 7. ECSIT Interacts with Mitophagy Regulators

(A and B) Coimmunoprecipitation (coIP) of (A) PINK1 with ECSIT and (B) ECSIT with PINK1 and western blot analysis of immunoprecipitated proteins and input lysate after overexpression in 293FT cells (ΔMLS, ECSIT lacking the MLS).

(C) CoIP of LC3b with ECSIT and western blot after overexpression in 293FT cells with or without CCCP for 1 hr (30 μM).

(D) Western blot analysis of ECSIT in lysates of WT IBMMs treated with LPS (100 ng/mL), CCCP (30 μM), or vehicle (DMSO) for the indicated times.

(E and F) Western blot analysis of proteins coimmunoprecipitated with anti-ECSIT or control antibody (immunoglobulin heavy chain [Ig]) in lysates of WT BMDMs (E) or IBMMs (F) treated with 10 nM Bafilomycin A1 (Ba1) for 5 hr and/or 20 μM of CCCP (CC) for 1 hr.

(G) IP of ECSIT and control IP (ctrl) and western blot analysis of immunoprecipitated ECSIT (top, long exposure; bottom, short exposure) and input lysate in WT IBMMs treated with LPS (100 ng/mL), CCCP (30 μM), BafA1 (10 nM), or vehicle (–) for 1 hr.

(H) IP of ubiquitinated proteins and western blot analysis for ECSIT after overexpression of ECSIT, Parkin, PINK1, and VSV-tagged ubiquitin in 293FT.

NDUFAF1 protein was completely absent in ECSIT knockdown cells, it appeared that levels of other CI components (i.e., NDUFS3) were unaffected, resulting in accumulation of a 500-kDa CI intermediate (Vogel et al., 2007). Surprisingly, in ECSIT KO macrophages, the 370-kDa subcomplex is not detected, and we observed loss of the NDUFS3 subunit, which is involved in the earliest steps of CI assembly (Guarani et al., 2014; Mckenzie and Ryan, 2010; Mimaki et al., 2012; Vartak et al., 2014). Furthermore, and in contrast to knockdown experiments, no CI intermediates were detected (Figures 3 and 4). ECSIT-deleted macrophages hence exhibit a more severe phenotype than previously observed with ECSIT knockdown approaches. These results suggest an essential role for ECSIT in CI assembly/stability in macrophages. Although NDUFAF1 is a well

described CI assembly factor, and ECSIT deletion leads to its disappearance, it is unlikely that the role of ECSIT in CI assembly is only to stabilize NDUFAF1 because NDUFAF1 knockdown leads to impaired CI assembly but not its complete disruption (Nouws et al., 2010; Vogel et al., 2007). In addition, we show that the reintroduction of NDUFAF1 in ECSIT-deleted cells does not restore normal levels of NDUFS3 protein, suggesting that NDUFAF1 alone is not sufficient to restore CI subunits. Moreover, although TIMMDC1 is involved in the membrane anchoring of the Q subcomplex containing NDUFS3, TIMMDC1-depleted cells did not show reduced levels of NDUFS3 or NDUFAF1 (Guarani et al., 2014), suggesting that the role of ECSIT in CI assembly is independent of TIMMDC1 as well. One possibility is that ECSIT has a role in stabilizing an early peripheral arm intermediate containing NDUFS3 by facilitating its anchoring in the membrane by ND1, for example (Guerrero-Castillo et al., 2017). It is important to highlight that ECSIT and NDUFS3 were co-purified by tandem affinity purification (TAP) tag and IP-MS, indicating a putative interaction between these proteins (Guarani et al., 2014; West et al., 2011).

The differences observed in our data and that of Vogel et al. (2007) might be due to the use of different cell types or due to the fact that previous experiments were performed using a knockdown approach. Importantly, nuclear encoded mRNA levels for NDUFAF1 and NDUFS3 and mitochondrially encoded ND6 mRNA levels were unchanged in ECSIT-deleted cells (Figure S4A), indicating that the regulation of CI disappearance is post-transcriptional. Mitochondria have a sophisticated quality control system that repairs or degrades misfolded, oxidized, or unassembled proteins. This system includes several mitochondrial chaperones and proteases besides the ubiquitin-proteasome system (UPS) (Heo and Rutter, 2011; Karbowski and Youle, 2011; Livnat-Levanon and Glickman, 2011). However, the UPS pathway and lysosomal degradation did not seem to be involved in the degradation of the CI subunits NDUFAF1 and NDUFS3 (Figure S4B). It is possible that the CI subunits are translocated and imported to the mitochondria to be degraded by mitochondrial proteases. It is important to note that some non-assembled OXPHOS subunits have been described as substrates for mitochondrial ATPases associated with diverse cellular activities (AAA) proteases (Arlt et al., 1996; Guzélin et al., 1996; Stiburek et al., 2012) and that LON/ClpP proteases have been shown to mediate degradation of CI under conditions of increased mROS production (Pryde et al., 2016).

Mitochondrial alterations in ECSIT-deleted macrophages lead to drastic effects on mitochondrial functions. Surprisingly, ATP levels were unaltered, suggesting that increased glycolysis compensates for lower ATP production by mitochondria. This is supported by a dramatic decrease in ATP levels upon inhibition of glycolysis in cells lacking ECSIT (Figure 3A). However, this metabolic shift is not a reprogramming phenomenon because mRNA levels of key glycolytic regulators and enzymes were not affected (Figure S3), and the mechanism of this increased flux is still unknown. Thus, without an increase in glycolytic capacity, we expect that ECSIT-deleted cells will be more sensitive to ATP-demanding stresses, and the function of cells like macrophages is likely to be altered *in vivo*, at sites of ongoing inflammation, for example.

We initially deleted ECSIT to confirm the role of ECSIT in the induction of mROS by TLRs upon phagocytosis of bacterial pathogens. Although the induction of mROS by bacterial products was abrogated in macrophages lacking ECSIT, this analysis was complicated by changes in baseline mROS production. Macrophages lacking ECSIT exhibit a significant increase in constitutive mROS production (Figure 5B). This is in agreement with other reports where deficiencies in CI subunits were studied (Jin et al., 2014; Miwa et al., 2014; Vogel et al., 2007). Given that CI is totally absent in ECSIT KO macrophages, it is likely that there might be another source of mROS in these cells. For example, complex III and, to a much lesser extent, CII have also been implicated in ROS production (Bolisetty and Jaimes, 2013; Casteilla et al., 2001; McLennan and Degli Esposti, 2000; Yankovskaya et al., 2003). Another possibility is the generation of ROS through alpha-KGDH (alpha-ketoglutarate dehydrogenase). It was reported that alpha-KGDH can produce ROS as a result of an increased NADH:NAD^+ ratio (Starkov et al., 2004; Tretter and Adam-Vizi, 2004), as observed in ECSIT-deleted cells (Figure 3E). Nevertheless, additional studies are necessary to understand the source of increased ROS in ECSIT KO macrophages because other enzymes have been implicated in ROS generation as well (Mrácek et al., 2009; Zorov et al., 2014).

Our previous study in macrophages revealed induction of mROS as a consequence of interaction of activated TLR signaling complexes containing TRAF6 with mitochondrial ECSIT (West et al., 2011). We observed a relocalization of ECSIT from the inner mitochondrial membrane to the OMM. Using knockdown approaches, we previously found that ECSIT was important for mitochondrial recruitment of TRAF6 and for inducible production of mROS in LPS-stimulated macrophages. The results obtained with ECSIT deletion in macrophages support an important role in the regulation of CI-dependent ROS (Figure 5) and suggest that this role may be secondary to regulation of CI assembly and protein stability. Therefore, these findings provide further support for the assertion that CI is the key source of mROS during bacterial phagocytosis.

It will be critical to explore the physiological relevance of the mechanisms elucidated here by examining the effects of ECSIT loss on innate immunity in *in vivo* models of infection. Based on our previous work (West et al., 2011), we expect that perturbed metabolism and mROS inducibility in ECSIT-deleted macrophages will impair resistance to bacterial infection. Moreover, multiple studies suggest that crosstalk between anti-bacterial autophagy and mitophagy (Randow and Youle, 2014) contributes to resistance to bacterial infection. Autophagy (Benjamin et al., 2013) and LC3-associated phagocytosis (Sarkar et al., 2017) have been shown to restrict *S. typhimurium* infection, and Parkin can contribute to resistance against *M. tuberculosis* and *S. typhimurium* (Manzanillo et al., 2013). Because we show that ECSIT is involved in mitophagy and that it interacts with LC3b, ECSIT loss might affect either or both of these pathways in addition to its expected effects on ROS production.

In summary, our results present ECSIT as a link between mitochondrial quality control, CI function, and mROS production in macrophages and reveal a unique homeostasis of CI in macrophages, which could be instrumental for macrophage function as suggested by Garaude et al. (2016).

EXPERIMENTAL PROCEDURES

Further details and an outline of resources used in this work can be found in the Supplemental Experimental Procedures.

Mice

Animals used for experiments were age-matched (8–12 weeks old) and sex-matched and were bred and housed under standard conditions in accordance with Columbia University Institutional Animal Care and Use Committee policies. All mouse protocols were approved by Columbia University. The *Ecsit*$^{f/f}$ mouse was generated following methods explained in the Supplemental Experimental Procedures (Yusa et al., 2011), backcrossed into the C57BL/6 background, and then bred to the Ecsit$^{+/-}$ (Xiao et al., 2003) and LysM-Cre (The Jackson Laboratory) or Rosa26Cre-ERT2 (B. Reizis, personal communication) mouse strains.

Cell Systems

BMDMs were harvested from 8- to 12-week-old ECSIT$^{f/-}$/LysM-Cre^{+} (WT) and ECSIT$^{+/+}$/LysM-Cre^{+} (cKO) or ECSIT$^{f/f}$/Cre-ERT2^{+} littermates and cultured for a period of 7 days in DMEM containing L929 conditioned medium. BMDMs from ECSIT$^{f/f}$/Cre-ERT2^{+} mice were treated with 4-hydroxy (4OH)-tamoxifen (500 nM) or vehicle on days 1, 3, and 6 of differentiation and plated for experiments on day 7. IBMMs from ECSIT$^{f/f}$/Cre-ERT2^{+} mice were treated with 500 nM of 4OH-tamoxifen or vehicle for 48 hr, washed, and cultured for 5–12 days prior to testing. These macrophages are referred to as iKO or WT, respectively. Relevance of the use of IBMMs was tested in assays performed in both BMDMs and IBMMs.

Statistical Analysis

Statistical analysis was conducted using GraphPad Prism 6 software. All data were tested for normal distribution of variables. Normally distributed data are displayed as means ± SD unless otherwise noted. Comparisons between two groups were performed with Student's t test when normally distributed or Mann-Whitney test otherwise. Groups of three or more were analyzed by one-way ANOVA or the Kruskal-Wallis test. Values of n for each experiment are reported in the figures and figure legends. $p < 0.05$ was considered significant. Statistical parameters for each experiment can be found in the figure legends.

SUPPLEMENTAL INFORMATION

Supplemental Information includes Supplemental Experimental Procedures and five figures and can be found with this article online at https://doi.org/10.1016/j.celrep.2018.02.051.

ACKNOWLEDGMENTS

We are grateful to Dr. B. Reizis and Dr. Thomas Ludwig for providing the Rosa26Cre-ERT2 mouse strain; Dr. R. Jaenisch and Dr. D. Trono for providing the plasmids used in lentivirus generation for IBMM transduction; Dr. N. Mizushima for the pMXs-IP HA-Parkin plasmid (Yoshii et al., 2011); Dr. M. Cookson for the pCMVTNT PINK1 C-myc plasmid (Beilina et al., 2005); Drs. P. Chastagner, A. Israel, and C. Brou for the pcDNA3 VSV-Ub plasmid; Dr. T. Meila for the YFP-LC3 plasmid; and Dr. Kosuke Yusa for the pMCS-DTA plasmid (Yusa et al., 2011). We thank Dr. Alexander Tzagoloff from Columbia University and Dr. Malgorzata Rak from Robert-Debré University Hospital for providing ATP synthase F1 alpha and beta subunits and ND6 antibodies, respectively, and Dr. Victor Lin from Columbia University for technical assistance and advice. We also thank Dr. Sujatha Gurunathan for help with writing the manuscript. The study was supported by grants from the NIH (AI33443 and ES025677) and institutional funds from Columbia University. A.L. was partly supported by EMBO Long-Term Fellowship ALTF-390-2012.

AUTHOR CONTRIBUTIONS

Conceptualization, F.R.G.C., A.L., M.S.H., and S.G.; Methodology, F.R.G.C., A.L., and S.G.; Investigation, F.R.G.C. and A.L.; Resources, J.J.S.; Writing – Original Draft, F.R.G.C., A.L., M.S.H., and S.G.; Writing – Review and Editing, A.L., M.S.H., and S.G.; Funding Acquisition, A.L. and S.G.

DECLARATION OF INTERESTS

The authors declare no competing interests.

Received: July 5, 2017
Revised: January 31, 2018
Accepted: February 12, 2018
Published: March 6, 2018

REFERENCES

Alston, C.L., Compton, A.G., Formosa, L.E., Strecker, V., Oláhová, M., Haack, T.B., Smet, J., Stouffs, K., Diakumis, P., Ciara, E., et al. (2016). Biallelic Mutations in TMEM126B Cause Severe Complex I Deficiency with a Variable Clinical Phenotype. Am. J. Hum. Genet. *99*, 217–227.

Andrews, B., Carroll, J., Ding, S., Fearnley, I.M., and Walker, J.E. (2013). Assembly factors for the membrane arm of human complex I. Proc. Natl. Acad. Sci. USA *110*, 18934–18939.

Arlt, H., Tauer, R., Feldmann, H., Neupert, W., and Langer, T. (1996). The YTA10-12 complex, an AAA protease with chaperone-like activity in the inner membrane of mitochondria. Cell *85*, 875–885.

Ashrafi, G., and Schwarz, T.L. (2013). The pathways of mitophagy for quality control and clearance of mitochondria. Cell Death Differ. *20*, 31–42.

Baertling, F., Sánchez-Caballero, L., van den Brand, M.A.M., Wintjes, L.T., Brink, M., van den Brandt, F.A., Wilson, C., Rodenburg, R.J.T., and Nijtmans, L.G.J. (2017). NDUFAF4 variants are associated with Leigh syndrome and cause a specific mitochondrial complex I assembly defect. Eur. J. Hum. Genet. *25*, 1273–1277.

Beilina, A., Van Der Brug, M., Ahmad, R., Kesavapany, S., Miller, D.W., Petsko, G.A., and Cookson, M.R. (2005). Mutations in PTEN-induced putative kinase 1 associated with recessive parkinsonism have differential effects on protein stability. Proc. Natl. Acad. Sci. USA *102*, 5703–5708.

Bénit, P., Beugnot, R., Chretien, D., Giurgea, I., De Lonlay-Debeney, P., Issartel, J.P., Corral-Debrinski, M., Kerscher, S., Rustin, P., Rötig, A., and Munnich, A. (2003). Mutant NDUFV2 subunit of mitochondrial complex I causes early onset hypertrophic cardiomyopathy and encephalopathy. Hum. Mutat. *21*, 582–586.

Benjamin, J.L., Sumpter, R., Jr., Levine, B., and Hooper, L.V. (2013). Intestinal epithelial autophagy is essential for host defense against invasive bacteria. Cell Host Microbe *13*, 723–734.

Bet, L., Bresolin, N., Moggio, M., Meola, G., Prelle, A., Schapira, A.H., Binzoni, T., Chomyn, A., Fortunato, F., Cerretelli, P., et al. (1990). A case of mitochondrial myopathy, lactic acidosis and complex I deficiency. J. Neurol. *237*, 399–404.

Bolisetty, S., and Jaimes, E.A. (2013). Mitochondria and reactive oxygen species: physiology and pathophysiology. Int. J. Mol. Sci. *14*, 6306–6344.

Breuer, M.E., Koopman, W.J., Koene, S., Nooteboom, M., Rodenburg, R.J., Willems, P.H., and Smeitink, J.A. (2013). The role of mitochondrial OXPHOS dysfunction in the development of neurologic diseases. Neurobiol. Dis. *51*, 27–34.

Casteilla, L., Rigoulet, M., and Pénicaud, L. (2001). Mitochondrial ROS metabolism: modulation by uncoupling proteins. IUBMB Life *52*, 181–188.

Fassone, E., Taanman, J.W., Hargreaves, I.P., Sebire, N.J., Cleary, M.A., Burch, M., and Rahman, S. (2011). Mutations in the mitochondrial complex I assembly factor NDUFAF1 cause fatal infantile hypertrophic cardiomyopathy. J. Med. Genet. *48*, 691–697.

Garaude, J., Acín-Pérez, R., Martínez-Cano, S., Enamorado, M., Ugolini, M., Nistal-Villán, E., Hervás-Stubbs, S., Pelegrín, P., Sander, L.E., Enríquez, J.A., and Sancho, D. (2016). Mitochondrial respiratory-chain adaptations in macrophages contribute to antibacterial host defense. Nat. Immunol. *17*, 1037–1045.

Geng, J., Sun, X., Wang, P., Zhang, S., Wang, X., Wu, H., Hong, L., Xie, C., Li, X., Zhao, H., et al. (2015). Kinases Mst1 and Mst2 positively regulate phagocytic induction of reactive oxygen species and bactericidal activity. Nat. Immunol. *16*, 1142–1152.

Guarani, V., Paulo, J., Zhai, B., Huttlin, E.L., Gygi, S.P., and Harper, J.W. (2014). TIMMDC1/C3orf1 functions as a membrane-embedded mitochondrial complex I assembly factor through association with the MCIA complex. Mol. Cell. Biol. *34*, 847–861.

Guerrero-Castillo, S., Baertling, F., Kownatzki, D., Wessels, H.J., Arnold, S., Brandt, U., and Nijtmans, L. (2017). The Assembly Pathway of Mitochondrial Respiratory Chain Complex I. Cell Metab. *25*, 128–139.

Guzélin, E., Rep, M., and Grivell, L.A. (1996). Afg3p, a mitochondrial ATP-dependent metalloprotease, is involved in degradation of mitochondrially-encoded Cox1, Cox3, Cob, Su6, Su8 and Su9 subunits of the inner membrane complexes III, IV and V. FEBS Lett. *381*, 42–46.

Heide, H., Bleier, L., Steger, M., Ackermann, J., Dröse, S., Schwamb, B., Zörnig, M., Reichert, A.S., Koch, I., Wittig, I., and Brandt, U. (2012). Complexome profiling identifies TMEM126B as a component of the mitochondrial complex I assembly complex. Cell Metab. *16*, 538–549.

Heo, J.M., and Rutter, J. (2011). Ubiquitin-dependent mitochondrial protein degradation. Int. J. Biochem. Cell Biol. *43*, 1422–1426.

Houshmand, M., Larsson, N.G., Oldfors, A., Tulinius, M., and Holme, E. (1996). Fatal mitochondrial myopathy, lactic acidosis, and complex I deficiency associated with a heteroplasmic A–> G mutation at position 3251 in the mitochondrial tRNALeu(UUR) gne. Hum. Genet. *97*, 269–273.

Jin, Z., Wei, W., Yang, M., Du, Y., and Wan, Y. (2014). Mitochondrial complex I activity suppresses inflammation and enhances bone resorption by shifting macrophage-osteoclast polarization. Cell Metab. *20*, 483–498.

Karbowski, M., and Youle, R.J. (2011). Regulating mitochondrial outer membrane proteins by ubiquitination and proteasomal degradation. Curr. Opin. Cell Biol. *23*, 476–482.

Kelly, B., Tannahill, G.M., Murphy, M.P., and O'Neill, L.A. (2015). Metformin Inhibits the Production of Reactive Oxygen Species from NADH:Ubiquinone Oxidoreductase to Limit Induction of Interleukin-1β (IL-1β) and Boosts Interleukin-10 (IL-10) in Lipopolysaccharide (LPS)-activated Macrophages. J. Biol. Chem. *290*, 20348–20359.

Kirby, D.M., Crawford, M., Cleary, M.A., Dahl, H.H., Dennett, X., and Thorburn, D.R. (1999). Respiratory chain complex I deficiency: an underdiagnosed energy generation disorder. Neurology *52*, 1255–1264.

Koene, S., Rodenburg, R.J., van der Knaap, M.S., Willemsen, M.A., Sperl, W., Laugel, V., Ostergaard, E., Tarnopolsky, M., Martin, M.A., Nesbitt, V., et al. (2012). Natural disease course and genotype-phenotype correlations in Complex I deficiency caused by nuclear gene defects: what we learned from 130 cases. J. Inherit. Metab. Dis. *35*, 737–747.

Kopp, E., Medzhitov, R., Carothers, J., Xiao, C., Douglas, I., Janeway, C.A., and Ghosh, S. (1999). ECSIT is an evolutionarily conserved intermediate in the Toll/IL-1 signal transduction pathway. Genes Dev. *13*, 2059–2071.

Leadsham, J.E., Sanders, G., Giannaki, S., Bastow, E.L., Hutton, R., Naeimi, W.R., Breitenbach, M., and Gourlay, C.W. (2013). Loss of cytochrome c oxidase promotes RAS-dependent ROS production from the ER resident NADPH oxidase, Yno1p, in yeast. Cell Metab. *18*, 279–286.

Lin, M.T., and Beal, M.F. (2006). Mitochondrial dysfunction and oxidative stress in neurodegenerative diseases. Nature *443*, 787–795.

Livnat-Levanon, N., and Glickman, M.H. (2011). Ubiquitin-proteasome system and mitochondria - reciprocity. Biochim. Biophys. Acta *1809*, 80–87.

Loeffen, J.L., Smeitink, J.A., Trijbels, J.M., Janssen, A.J., Triepels, R.H., Sengers, R.C., and van den Heuvel, L.P. (2000). Isolated complex I deficiency in children: clinical, biochemical and genetic aspects. Hum. Mutat. *15*, 123–134.

Manzanillo, P.S., Ayres, J.S., Watson, R.O., Collins, A.C., Souza, G., Rae, C.S., Schneider, D.S., Nakamura, K., Shiloh, M.U., and Cox, J.S. (2013). The ubiquitin ligase parkin mediates resistance to intracellular pathogens. Nature *501*, 512–516.

Mckenzie, M., and Ryan, M.T. (2010). Assembly factors of human mitochondrial complex I and their defects in disease. IUBMB Life *62*, 497–502.

McLennan, H.R., and Degli Esposti, M. (2000). The contribution of mitochondrial respiratory complexes to the production of reactive oxygen species. J. Bioenerg. Biomembr. *32*, 153–162.

Mimaki, M., Wang, X., McKenzie, M., Thorburn, D.R., and Ryan, M.T. (2012). Understanding mitochondrial complex I assembly in health and disease. Biochim. Biophys. Acta *1817*, 851–862.

Miwa, S., Jow, H., Baty, K., Johnson, A., Czapiewski, R., Saretzki, G., Treumann, A., and von Zglinicki, T. (2014). Low abundance of the matrix arm of complex I in mitochondria predicts longevity in mice. Nat. Commun. *5*, 3837.

Mrácek, T., Pecinová, A., Vrbacký, M., Drahota, Z., and Houstek, J. (2009). High efficiency of ROS production by glycerophosphate dehydrogenase in mammalian mitochondria. Arch. Biochem. Biophys. *481*, 30–36.

Narendra, D., Tanaka, A., Suen, D.F., and Youle, R.J. (2008). Parkin is recruited selectively to impaired mitochondria and promotes their autophagy. J. Cell Biol. *183*, 795–803.

Narendra, D.P., Jin, S.M., Tanaka, A., Suen, D.F., Gautier, C.A., Shen, J., Cookson, M.R., and Youle, R.J. (2010). PINK1 is selectively stabilized on impaired mitochondria to activate Parkin. PLoS Biol. *8*, e1000298.

Nouws, J., Nijtmans, L., Houten, S.M., van den Brand, M., Huynen, M., Venselaar, H., Hoefs, S., Gloerich, J., Kronick, J., Hutchin, T., et al. (2010). Acyl-CoA dehydrogenase 9 is required for the biogenesis of oxidative phosphorylation complex I. Cell Metab. *12*, 283–294.

Pagano, G., Talamanca, A.A., Castello, G., Cordero, M.D., d'Ischia, M., Gadaleta, M.N., Pallardó, F.V., Petrović, S., Tiano, L., and Zatterale, A. (2014). Oxidative stress and mitochondrial dysfunction across broad-ranging pathologies: toward mitochondria-targeted clinical strategies. Oxid. Med. Cell. Longev. *2014*, 541230.

Petruzzella, V., and Papa, S. (2002). Mutations in human nuclear genes encoding for subunits of mitochondrial respiratory complex I: the NDUFS4 gene. Gene *286*, 149–154.

Pitkanen, S., and Robinson, B.H. (1996). Mitochondrial complex I deficiency leads to increased production of superoxide radicals and induction of superoxide dismutase. J. Clin. Invest. *98*, 345–351.

Pryde, K.R., Taanman, J.W., and Schapira, A.H. (2016). A LON-ClpP Proteolytic Axis Degrades Complex I to Extinguish ROS Production in Depolarized Mitochondria. Cell Rep. *17*, 2522–2531.

Randow, F., and Youle, R.J. (2014). Self and nonself: how autophagy targets mitochondria and bacteria. Cell Host Microbe *15*, 403–411.

Sarkar, A., Tindle, C., Pranadinata, R.F., Reed, S., Eckmann, L., Stappenbeck, T.S., Ernst, P.B., and Das, S. (2017). ELMO1 Regulates Autophagy Induction and Bacterial Clearance During Enteric Infection. J. Infect. Dis. *216*, 1655–1666.

Sazanov, L.A. (2015). A giant molecular proton pump: structure and mechanism of respiratory complex I. Nat. Rev. Mol. Cell Biol. *16*, 375–388.

Starkov, A.A., Fiskum, G., Chinopoulos, C., Lorenzo, B.J., Browne, S.E., Patel, M.S., and Beal, M.F. (2004). Mitochondrial alpha-ketoglutarate dehydrogenase complex generates reactive oxygen species. J. Neurosci. *24*, 7779–7788.

Stiburek, L., Cesnekova, J., Kostkova, O., Fornuskova, D., Vinsova, K., Wenchich, L., Houstek, J., and Zeman, J. (2012). YME1L controls the accumulation of respiratory chain subunits and is required for apoptotic resistance, cristae morphogenesis, and cell proliferation. Mol. Biol. Cell *23*, 1010–1023.

Tretter, L., and Adam-Vizi, V. (2004). Generation of reactive oxygen species in the reaction catalyzed by alpha-ketoglutarate dehydrogenase. J. Neurosci. *24*, 7771–7778.

Vartak, R.S., Semwal, M.K., and Bai, Y. (2014). An update on complex I assembly: the assembly of players. J. Bioenerg. Biomembr. *46*, 323–328.

Vogel, R.O., Janssen, R.J., van den Brand, M.A., Dieteren, C.E., Verkaart, S., Koopman, W.J., Willems, P.H., Pluk, W., van den Heuvel, L.P., Smeitink, J.A., and Nijtmans, L.G. (2007). Cytosolic signaling protein Ecsit also localizes to mitochondria where it interacts with chaperone NDUFAF1 and functions in complex I assembly. Genes Dev. *21*, 615–624.

Wen, H., Ma, H., Cai, Q., Lin, S., Lei, X., He, B., Wu, S., Wang, Z., Gao, Y., Liu, W., et al. (2018). Recurrent ECSIT mutation encoding V140A triggers hyperinflammation and promotes hemophagocytic syndrome in extranodal NK/T cell lymphoma. Nat. Med. *24*, 154–164.

West, A.P., Brodsky, I.E., Rahner, C., Woo, D.K., Erdjument-Bromage, H., Tempst, P., Walsh, M.C., Choi, Y., Shadel, G.S., and Ghosh, S. (2011). TLR signalling augments macrophage bactericidal activity through mitochondrial ROS. Nature *472*, 476–480.

Xiao, C., Shim, J.H., Klüppel, M., Zhang, S.S., Dong, C., Flavell, R.A., Fu, X.Y., Wrana, J.L., Hogan, B.L., and Ghosh, S. (2003). Ecsit is required for Bmp signaling and mesoderm formation during mouse embryogenesis. Genes Dev. *17*, 2933–2949.

Yankovskaya, V., Horsefield, R., Törnroth, S., Luna-Chavez, C., Miyoshi, H., Léger, C., Byrne, B., Cecchini, G., and Iwata, S. (2003). Architecture of succinate dehydrogenase and reactive oxygen species generation. Science *299*, 700–704.

Yoshii, S.R., Kishi, C., Ishihara, N., and Mizushima, N. (2011). Parkin mediates proteasome-dependent protein degradation and rupture of the outer mitochondrial membrane. J. Biol. Chem. *286*, 19630–19640.

Yusa, K., Zhou, L., Li, M.A., Bradley, A., and Craig, N.L. (2011). A hyperactive piggyBac transposase for mammalian applications. Proc. Natl. Acad. Sci. USA *108*, 1531–1536.

Zorov, D.B., Juhaszova, M., and Sollott, S.J. (2014). Mitochondrial reactive oxygen species (ROS) and ROS-induced ROS release. Physiol. Rev. *94*, 909–950.

Cell Reports, Volume *22*

Supplemental Information

An Essential Role for ECSIT in Mitochondrial Complex I Assembly and Mitophagy in Macrophages

Flávia R.G. Carneiro, Alice Lepelley, John J. Seeley, Matthew S. Hayden, and Sankar Ghosh

Supplemental Figures

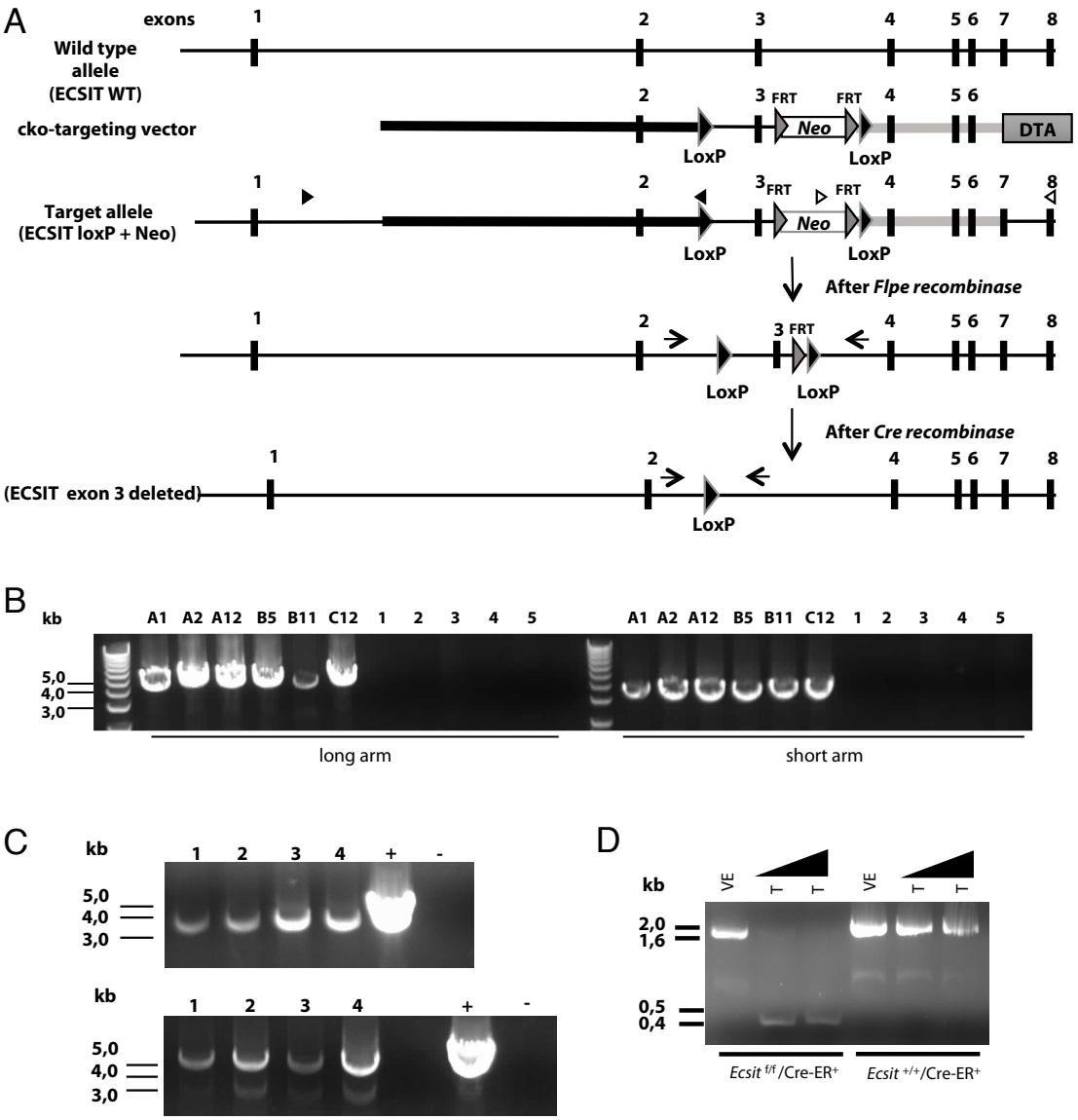

Figure S1. Construction of *Ecsit* conditional knockout mouse (cKO). ***Related to Figure 1.***
(A) Schematic representation of *Ecsit* cKO mouse generation. Exon 3 was flanked by 2 loxP sites and excised after conditional Cre expression. Thick black line: long arm; thick grey line: short arm. (B) Identification of correctly targeted embryonic stem (ES) cell clones by PCR. Correctly targeted ES cells (cKO allele) generated a 4.8 kb band (long arm recombination) and 3.7 kb band (short arm recombination). A1, A2, A12, B5, B11, and C12: ES clones. 1 to 5: PCR negative controls; templates used: 1- no DNA added; 2- cKO-targeting vector; 3- cKO-targeting vector in addition to WT black 6 mouse genomic DNA; 4- cKO-targeting vector in addition to WT black 6 ES cell lysate; 5- WT black 6 mouse genomic DNA. (C) Identification of *Ecsit* conditional allele in F1 line. Transmission through the chimeras germline to F1 was checked by PCR. DNA was extracted from the tails and used for amplification. Top, detection of the short arm (3.7 kb); Bottom, detection of the long arm (4.8 kb). 1-4: samples from 4 independent pups; + (Positive control): genomic DNA obtained from positive ES cell used as a template; - (Negative control): genomic DNA from WT black 6 mouse used as a template**.** (D) Detection of ECSIT deletion by PCR in Cre-ERT2^{+}/ECSIT$^{f/f}$ and E Cre-ERT2^{+}/ECSIT$^{+/+}$ mice. Bone marrow derived macrophages were treated for 7 days with 3 doses (days 1, 3 and 6 of differentiation) of 100 nM or 500 nM tamoxifen (T) or vehicle (VE). DNA was prepared at day 7 and tested by PCR. FRT: *DNA recognition site for Flpe* recombinase; DTA: diphtheria toxin A chain gene.

VE: vehicle; T: Tamoxifen treatment. Black arrow heads and open arrow heads: primers alignment positions for long arm and short arm amplifications by PCR, respectively. Arrows: primers to detect exon 3 deletion after Cre recombination.

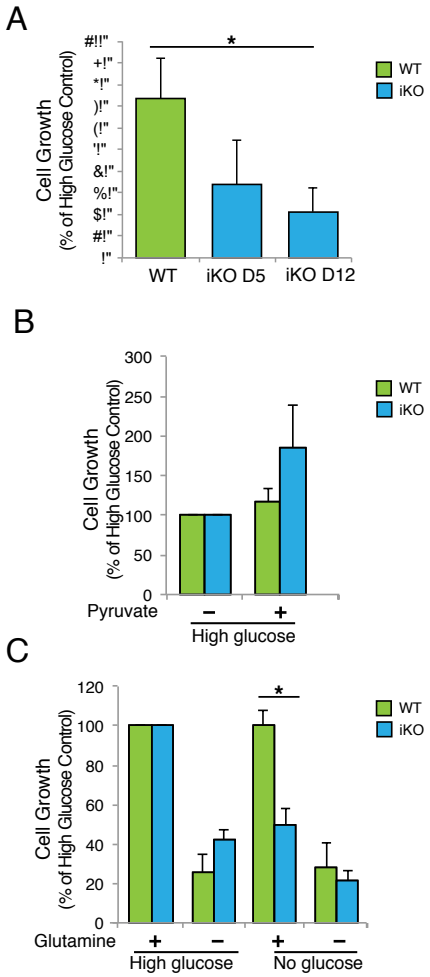

Figure S2. Metabolic adaptations in macrophage cells lacking ECSIT. ***Related to Figure 2.***
(A) Assessment of cell growth by crystal violet staining of IBMM 5 or 12 days after tamoxifen treatment. IBMM cultures were treated with 40 mM Sodium Oxamate for 24 h (n=3). (B, C) Cell growth by crystal violet staining of IBMM 12 days after Tamoxifen treatment initiation and maintained for 48 h in DMEM without or with 25 mM Glucose, 2 mM Sodium Pyruvate, 4 mM L-Glutamine (n=3). Means +/- SD of n experiments. *: $p<0.05$ in T-test.

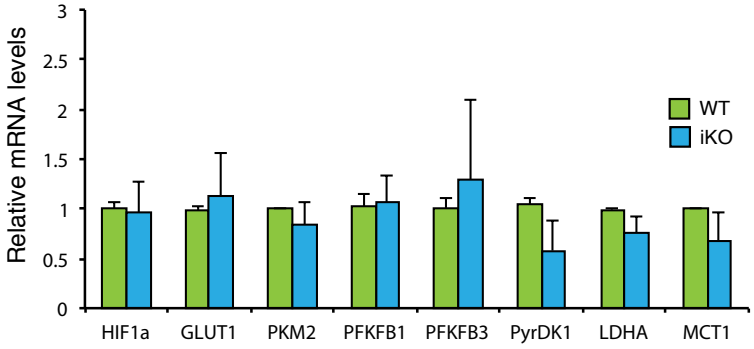

Figure S3. Metabolic shift in ECSIT-deleted macrophages is independent of transcriptional changes. ***Related to Figure 2***

Expression of transcripts relevant to the metabolic shift observed in ECSIT-deleted macrophages analyzed by RT-qPCR in WT and iKO IBMM 7 days after deletion induction by Tamoxifen, HPRT used as internal control.

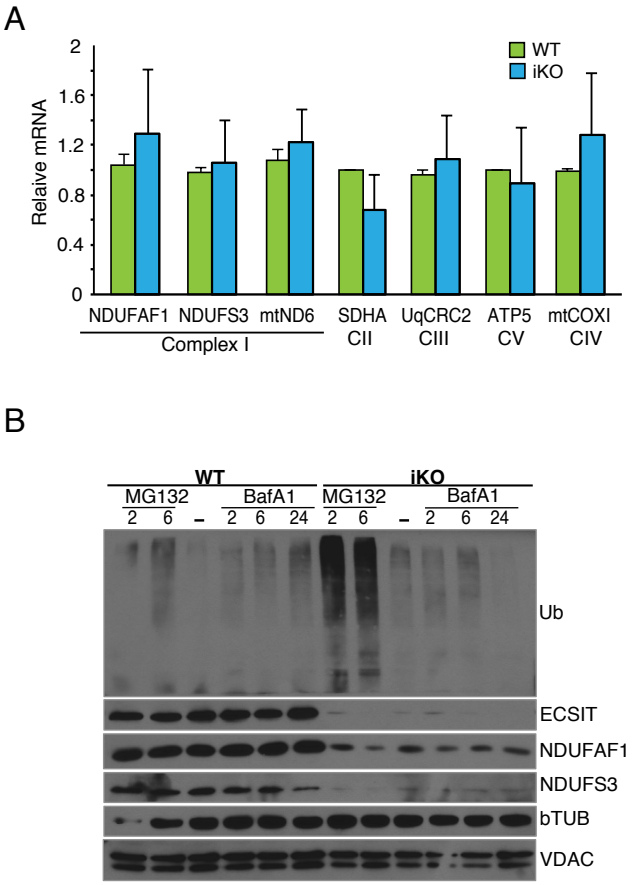

Figure S4. Loss of Complex I subunits in ECSIT-deleted macrophages is independent of transcriptional regulation and proteasomal and lysosomal degradation pathways. ***Related to Figure 4***

(A) Complex I subunits expression analyzed by RT-qPCR in WT and iKO IBMM 7 days after deletion induction, HPRT used as internal control. (B) WT or iKO macrophages treated with 10 µM MG132 or 10 nM Bafilomycin A1 (BafA1) for indicated time in hours. Total cell lysates were fractioned by SDS-PAGE and subjected to western blot analysis using antibodies against Ubiquitin (Ub), ECSIT, NDUFAF1, NDUFS3, beta Tubulin (bTUB) and VDAC1.

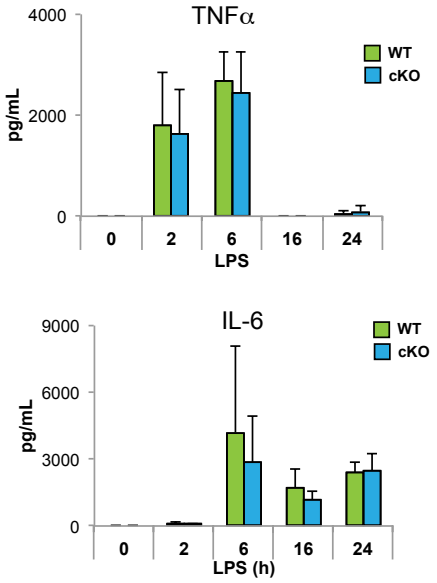

Figure S5. LPS response in macrophages lacking ECSIT. ***Related to Figure 5***
ELISA titration of IL-6 and TNFα release by cultured BMDM of the indicated genotype, following stimulation with 100 ng/mL LPS for the indicated times in hours.

Supplemental Experimental Procedures

Experimental Model Details

Mice

Animals used for experiments were age- (8-12 weeks old) and sex-matched and were bred and housed under standard conditions in accordance with Columbia University Institutional Animal Care and Use Committee policies. All mouse protocols were approved by Columbia University. The *Ecsit*$^{f/f}$ mouse was generated following the methods explained in corresponding Method Details section below and backcrossed into C57BL/6 background and then bred to Ecsit$^{+/-}$ (Xiao et al., 2003) and LysM-Cre (The Jackson Laboratory) or Rosa26Cre-ERT2 (from Dr. B. Reizis, made by Dr. T. Ludwig (unpublished)) mouse strains to produce Ecsit$^{f/-}$/LysM-Cre^{+} and Ecsit$^{+/+}$/LysM-Cre^{+} or Ecsit$^{f/f}$/Cre-ERT2^{+}, respectively.

Cell lines and primary cell cultures

L929 cells were obtained from American Type Culture Collection (ATCC CCL-1) and are of male origin. 293FT cells were obtained from ThermoScientific (R70007) and are suggested to be of female origin. ψCREJ2 cells (a kind gift of KA Fitzgerald) were used to produce J2 v-myc/v-raf transforming retrovirus (Xiao et al., 2012) (Blasi et al., 1987). Cell lines were plated in tissue culture dishes and maintained in standard culture media composed of DMEM (Gibco) medium supplemented with 10 % fetal bovine serum (FBS), penicillin (100 U/mL) and streptomycin (100 µg/mL).

L929 conditioned media was prepared from the supernatant of a 7-day culture of L929 cells. Harvested supernatant was clarified by centrifugation at 1500 rpm for 5 min and filtered. Bone marrow derived macrophages (BMDM) were harvested from 8-12-week old ECSIT$^{f/-}$/LysM-Cre^{+} (cKO) and ECSIT$^{+/+}$/LysM-Cre^{+}(WT) or ECSIT$^{f/f}$/Cre-ERT2^{+} littermates, plated and cultured on 15 cm Petri dishes for a period of 7 days in DMEM containing 10 % FBS, penicillin (100 U/mL) and streptomycin (100 µg/mL) plus 30 % L929 conditioned media. On day 7, cells were lifted from plates by incubation in PBS containing 1 mM EDTA for 5 minutes at 4°C and replated in multi-well plates

depending on the experiment. BMDMs from ECSIT$^{f/f}$/Cre-ERT2^{+} mice were treated with 4OH-Tamoxifen (500 nm) or ethanol vehicle on days 1, 3 and 6 of differentiation and plated for experiments at day 7. Thioglycollate elicited peritoneal macrophages were prepared as previously described (Rao et al., 2010). In summary, 2 ml of 3 % thioglycollate was injected into the peritoneal cavity and, after 3 days, peritoneal exudates were collected in cold PBS. Cells were washed twice in PBS and suspended in RPMI 1640 10 % FBS with penicillin (100 U/ml) and streptomycin (100 µg/ml) and allowed to rest overnight.

Macrophage immortalization was performed by infection of BMDM from an ECSIT$^{f/f}$/Cre-ERT2^{+} male mouse with J2 recombinant retrovirus according to Blasi et al., 1989 (Blasi et al., 1989). Briefly, 0.45-micron-filtered supernatants from cultured ψCREJ2 cells were added to harvested BMDMs at Day 1 for 16-24 h. Cells were washed with PBS and allowed to rest for an additional 16-24 h. Then, a second round of infection was performed. Cells were then maintained in culture for a few weeks in DMEM containing 10% FBS, penicillin, streptomycin and 30 % of L929 conditioned media and monitored for growth. Immortalized bone marrow derived macrophages (IBMM) from ECSIT$^{f/f}$/Cre-ERT2^{+} mouse were treated with 500 nM of 4OH-tamoxifen (Sigma H6278) (iKO) or vehicle (100 % Ethanol) (WT) for 48 h, washed away and cultured for 5 days prior to testing. For cell growth assay, cells were analyzed 5 or 12 days after tamoxifen treatment initiation. IBMM transduced with Tet inducible vector were cultured with 10 % Tet System approved FBS (Takara) instead of standard FBS.
Relevance of the use of IBMM was tested in some assays performed in both BMDM and IBMM. When indicated, IBMM were cultured in restricted culture media as described in Method Details below.

All cells were cultured in a humidified incubator at 37°C in a 5 % CO_2 atmosphere.

Method Details

***Ecsit* conditional knockout mouse**
To examine the effect of ECSIT deficiency *in vivo*, we have generated *Ecsit* conditional knockout animals (cko or *Ecsit*$^{f/f}$) by flanking exon 3 with 2 *LoxP* sites, through a method for constructing cko-targeting vectors using *E. coli* recombineering (Liu et al., 2003) (Fig S1A). After conditional Cre expression, a 1.3 kb-fragment of the *Ecsit* gene that includes exon 3 was deleted. The junction of exon 2 and 4 generated a premature STOP codon such that only a truncated protein consisting of the first 32 amino acids of ECSIT should be produced upon Cre mediated deletion. The *E. coli* SW106 strain (Liu et al., 2003) was transformed with a BAC encompassing the *Ecsit* gene and used to perform all the homologous recombination steps to introduce the floxed Neomycin resistance (*NeoR*) cassette into *Ecsit* gene. This strain can efficiently carry out homologous recombination between short terminal homology regions on a linear PCR-derived DNA fragment and sequences on a recipient DNA. The first recombination step was performed using a linear DNA fragment generated by PCR containing short terminal homology regions (60 bp) introduced by the primers LNeoL-intron3F and LNeoL-intron3R (table below) and the vector pL452 (Liu et al., 2003) as a template. The *NeoR* gene was subsequently removed via Cre recombinase. The removal of the floxed *NeoR* gene leaved a single *loxP* site at the target locus. The following step was the introduction of the second *loxP* site into the BAC. We used the cassette from pL451 vector that contains a FRT site upstream of *NeoR*, and *FRT* and *loxP* sites downstream of *NeoR* (Liu et al., 2003) and the primers FNeoFL-intron4F and FNeoFL-intron4R (table below) to generate the linear DNA fragment by PCR. The last step before the electroporation of the modified *Ecsit* fragment into the ES cell was the generation of the final cko-targeting vector containing the two flanking homology arms (long arm and short arm) for homologous recombination into the ES genome. This vector was generated through homologous recombination between the PCR product using the primers Ret-left1-ECSIT and Ret-right1-ECSIT (table below) and the vector pMCS-DTA (gift from Dr. Kosuke Yusa, Wellcome Trust Sanger Institute, (Yusa et al., 2011)) as a template and the BAC containing the floxed *Ecsit* exon 3. The cko-targeting vector was subsequently linearized and electroporated into 129B6 hybrid ES cells (Transgenic mouse facility at Columbia HICCC). Homologous recombination between cko-targeting vector and the ES genome was checked by PCR (Fig S1A,B). The primers long-arm2F and L83loxP (table below) to check the long arm integration were designed to anneal into the first *loxP* site and outside of the recombination arm, generating a DNA fragment of 4.8 kb. The second pair of primers ARM2/F2 and short-arm1R, to check the short arm integration, targeted a region inside of the *NeoR* gene and outside of the recombination arm and amplify a DNA fragment of 3.7 kb (Fig S1A,B). Chimeras were mated to C57BL/6 to test for germline transmission. Germline transmission was checked by PCR using the same pairs of primers used to check the positive ES cells (Fig S1C). DNA located between the two *FRT* sites was

removed by breeding these mice to a mouse strain expressing *Flpe* (ACTB-FLPe, from Jackson Laboratory). In this case, single *FRT* and single *loxP* sites were left behind at the targeted locus. To verify the success of the deletion strategy, ECSIT cko mice were crossed with Cre-ERT2 mice, in which Cre recombinase activity can be induced by tamoxifen, to excise the entire DNA between the *loxP* sites located on either side of *Ecsit* exon 3. Exon 3 deletion was checked by PCR using primers ECSIT-intron3F and ECSIT-intro4R (table below) generating a 425 bp-fragment after deletion and 1800 bp-fragment for the non-deleted gene (Fig S1A,D). ECSIT expression was successfully abrogated following *in vitro* tamoxifen treatment of $ECSIT^{f/f}$/Cre-$ERT2^{+}$ bone marrow-derived macrophages (BMDM) (Figure 1A, Fig S1D). We also crossed $ECSIT^{f/f}$ mice with LysM-Cre mice to delete ECSIT in the myeloid lineage. For more efficient deletion in primary macrophages, we bred $ECSIT^{f/+}$/LysM-Cre^{+} mice with $ECSIT^{+/-}$ heterozygous mice (Xiao, 2003), generating $ECSIT^{f/-}$/LysM-Cre^{+}, containing one KO allele and one floxed allele. $ECSIT^{+/+}$/LysM-Cre^{+} and $ECSIT^{f/-}$/LysM-Cre^{+} cells will be represented as WT and cKO, respectively.

Phenotyping of myeloid cells in mice with ECSIT deleted in macrophages

8-12 weeks old $ECSIT^{+/+}$/LysM-Cre^{+} and $ECSIT^{f/-}$/LysM-Cre^{+} were sacrificed by CO_2 asphyxia. Peritoneal cells were harvested with 5 mL PBS. 2 brachial and 2 inguinal lymph nodes were harvested, cut and incubated in digestion solution (20 µg/mL DNase I and 10 µg/mL Collagenase (Sigma-Aldrich) in DMEM (Invitrogen)) for 30 min at 37°C. Spleens were infused with digestion solution and incubated for 30-45 min at 37°C. Remaining tissues were further dilacerated on a 70 µm strainer, rinsed with cold PBS, 5 mM EDTA, centrifuged at 1500 rpm for 6 min, resuspended in Red Blood Cell lysis buffer (Sigma-Aldrich) and incubated at 37°C for 2 min. Lungs were dissected, cut and incubated in digestion solution for 30-45 min at 37°C. Remaining tissues were further dilacerated on a 70 µm strainer, rinsed with cold PBS, 5 mM EDTA, centrifuged at 1,500 rpm for 6 min, resuspended in 36 % Percoll (Sigma-Aldrich) in PBS and centrifuged at 2,500 rpm for 15 min at 20°C with slow acceleration and deceleration. Pellet was collected and resuspended in PBS, 5 mM EDTA, centrifuged and red blood cells were lysed as described above. One tibia bone was dissected and bone marrow cells flushed out with 2 mL PBS 3 % FCS, passed through a 70 µm strainer, rinsed with PBS 3 % FCS and red blood cells were lysed as described above. Centrifuged isolated cells were resuspended in PBS 3 % FCS and counted for cellularity. For phenotyping, around 3.10^{6} cells per staining were incubated with Fc blocking antibody 2.4G2 (1/2000, Tonbo) in PBS 3 % FCS for 1 h at 4°C. Cells were centrifuged and incubated with surface antibody: F4/80-FITC (1/100, eBiosciences, BM8), CD11b-PE (1/400, 1/700 for peritoneal cavity, eBiosciences, M1/70), Ly6G-VF405 (1/200, Tonbo, 1A8), CD3-PerCPCy5.5 (1/100, Tonbo, 145-2C11), B220-APC780 (1/200, eBiosciences, RA3-6B2) for 1h at 4°C. Cells were washed and resuspended in PBS 3 % FCS with 1 µg/mL DAPI (Sigma-Aldrich), to exclude dead cells. Stained cells were analyzed by flow cytometry on an LSRII and data analysis was performed using FlowJo software. Macrophages were defined as CD11b+, F4/80+ and monocytes as CD11b+, F4/80- in lineage negative (CD3-, B220-, Ly6G-) cells.

Cellular fractionation, mitochondrial isolation

iBMM and BMDM from 2-3 15 cm-Petri dishes were washed twice in PBS and detached in TEN buffer (40 mM Tris-HCl pH 7.4, 150 mM NaCl, 1 mM EDTA) for 5 min at 4°C. Cells were centrifuged and cell pellets were re-suspended in ten pellet volumes of RSB buffer (10 mM NaCl, 1.5 mM $CaCl_2$, 10 mM Tris-HCl, pH 7.5), swelled on ice for 10 min, homogenized with a dounce homogenizer, then 2.5× MS buffer (525 mM mannitol, 175 mM sucrose, 12.5 mM Tris-HCl, pH 7.5, 12.5 mM EDTA) was added to 1× final buffer concentration. The homogenate was centrifuged three times at 980*g* for 10 min to pellet nuclei. The supernatant was transferred to a fresh tube, an aliquot taken for total lysate sample and remaining supernatant spun at 17,000*g* for 30 min to pellet mitochondria. Supernatant consisted of cytosol fraction. The mitochondrial pellet was washed three times with 1× MS buffer, by centrifugation at 13,000 rpm for 10 min.

Purified mitochondria proteins were then solubilized with specific detergents according to the different purposes or resuspended in 1× MS with 10 % glycerol, flash frozen in liquid nitrogen and stored at -80°C. For SDS-PAGE, mitochondrial pellets were re-suspended in SDS lysis buffer (20 mM Tris-HCl, 1% SDS, pH 7.5). Protein concentrations were determined using the microBCA protein kit (Thermo Scientific).

For complex I assay, mitochondrial protein extraction was performed according the manufacturer's instructions. For blue native gel, mitochondrial complexes were prepared as previously described using DDM detergent (dodecylmaltoside) (Wittig et al., 2006). Briefly, 400 µg of purified mitochondria were solubilized in 40 µL of 50 mM NaCl, 50 mM bis-tris HCl pH 7.0, 2 mM aminohexanoic acid, 1.0 mM EDTA, 2 % DDM, incubated on ice for 5 min and centrifuged for 20 min at 20,000g. Supernatants were collected and protein concentration determined. Samples were prepared by adding 4× native gel sample buffer (0.1 % Ponceau S, 50 % glycerol, (wt/vol)) to final 1×

concentration and 2.5 µL of additive (5 % (wt/vol) Coomassie blue G-250 (Serva) in 500 mM 6-aminohexanoic acid).

Blue Native Gel Electrophoresis and transfer and in-gel complex I activity assay
100-150 µg solubilized mitochondrial complexes and 5 µL Native marker (Invitrogen) were loaded on a NativePAGE 4-16 % Bis-Tris Protein gel (Invitrogen) and gels were run for 30 min at 30 V and then overnight at 80 V at 4°C according to Nijtmans et al (Nijtmans et al., 2002) and following the manufacturer's instructions. Anode buffer (50 mM Bis-Tris, 50 mM Glycine pH 7) and dark blue cathode buffer (anode buffer with 0.02% Coomassie Blue G-250) were replaced by light blue cathode buffer (anode buffer with 0.002% Coomassie Blue G-250) when sample buffer reached 1/3 of the gel. Gels were either stained for proteins using Imperial Protein Stain (ThermoScientific) for 1 h and destained overnight, or transferred for immunoblotting, or processed for in-gel activity. For immunoblotting, complexes were transferred to PVDF according to Diaz et al (Diaz et al., 2009). Gels were incubated in anode buffer with 0.1 % SDS for 15 min. Wet transfer was performed in transfer buffer (143 mM glycine, 19 mM Tris Base) with 10% Methanol and 0.05 % SDS overnight at 30 V at 4°C. Membranes were dried and destained quickly with methanol before immunoblotting. In-gel Complex I activity was performed according to Diaz et al (Diaz et al., 2009). Gel was washed 3 times in 0.1 M Tris pH 7.4 and then incubated in 0.1 M Tris, 1 mg/mL NBT (nitro blue tetrazolium), 0.14 mM NADH for 2 h. Gel was then destained in 25 % Methanol, 10% Acetic Acid in water overnight.

Lactate, NADH, Complex I and ATP assays
L-lactate was measured at indicated time points on cellular supernatants from macrophage cultures non stimulated or stimulated with E. *coli* LPS (100 ng/mL) using L-lactate assay Kit I (Eton Bioscience). For complex I NADH dehydrogenase activity, WT and ECSIT-deleted iBMM were treated with vehicle (70 % Ethanol) or chloramphenicol (Sigma-Aldrich) for 5 days at a final concentration of 20 µg/mL before harvesting cells. Crude mitochondrial extracts were then assessed using a Complex I Enzyme Activity Microplate Assay kit (Abcam). Total cell lysate was analyzed for NADH/NAD^+ ratio using NAD^+/NADH quantification colorimetric kit (BioVision). ATP levels were determined using the ATPlite™ Luminescence Assay System (Perkin Elmer). When indicated, cells were pretreated for 4 h with 50 mM 2-DG (2-deoxyglucose). ATP levels were normalized to cell numbers. All the measurements were performed according to the manufacturer's instructions.

ROS, mitochondrial mass and mitochondrial potential measurements
Cells were plated at 300,000 cells/well in non-treated 6-well plates and treated with E. *coli* LPS (100 ng/mL), Rotenone (1 µM), Antimycin A1 (5 µM) or vehicle (DMSO) for 20 min (Sigma-Aldrich). Culture medium was removed, cells washed with PBS, then incubated with MitoSOX (Invitrogen) to measure mROS superoxide or chloromethyl derivative of 2',7'-dichlorodihydrofluorescein diacetate (CM-H_2DCFDA) to measure total ROS at 2.5 µM final concentration in serum-free OPTIMEM (Invitrogen) for 15 to 30 min at 37°C. Cells were washed with warm PBS, removed from plates with TEN buffer (40 mM Tris-HCl pH 7.4, 150 mM NaCl, 1 mM EDTA) by pipeting, pelleted and resuspended in cold PBS containing 1% FBS for FACS analysis. To analyze the mitochondrial potential and mitochondrial mass, IBMM and BMDM were seeded at 150,000 cells/well in a non-treated 12-well plate, treated with CCCP for 15mn (30 µM) and stained with 50 nM TMRM (Tetramethylrhodamine, Methyl Ester, Perchlorate, Invitrogen) or Mitotracker Green FM (Invitrogen) for 45 min at 37°C. For each condition, unstained controls were treated similarly, except that dyes were replaced by vehicle (DMSO). Mitochondrial ROS, potential and mass were analyzed by flow cytometry on a Fortessa or LSRII cytometer (BD). Data analysis was performed using FlowJo software and fluorescence from unstained controls was subtracted from respective stained samples. MFI: mean fluorescence intensity.

ELISA
Cells were plated at 300,000 cells/well in non-treated 6-well plates and treated with E. *coli* LPS (100 ng/mL) for indicated times. Supernatant were harvested and clarified and cytokine levels were assessed with mouse IL-6 and TNFα ELISA kits (BD Biosciences), following the manufacturer's protocol.

Cell growth
8,000 cells were plated in flat bottom 96-well plates in DMEM without glucose (Invitrogen) supplemented with 10 % FBS, 20 ng/mL M-CSF (R&D) and 25 mM glucose (Sigma, High Glucose condition) or 10 mM galactose (Sigma). 40 mM Sodium Oxamate (Sigma) was added to inhibit LDH. In other conditions, DMEM without glucose,

nor glutamine (Invitrogen) was used with addition of 25 mM glucose (Sigma, High Glucose condition), 2 mM Sodium Pyruvate (Invitrogen) or 4 mM L-Glutamine (Invitrogen).
24 or 48 hours later, cells were washed once with PBS, fixed in 4% PFA in PBS for 15 min, washed once with water and stained with 0.1 % crystal violet for 20 min. Cells were washed three times with water and allowed to dry. Retained crystal violet was solubilized in 100 % methanol and OD read at 595 nm.

RT-PCR and qPCR
Total RNA was prepared using Rneasy minikit (Qiagen) according to manufacturer's protocol and RNA purity and quantity were analyzed by photometry (Gen5 BioTek). For cDNA synthesis, 2 µg total RNA were reverse transcribed in cDNA using Superscript III enzyme and oligo dT (Invitrogen). Quantitative PCR (qPCR) was performed using SYBR Green (Quanta) and primers as listed in table below. Differences in cDNA inputs were corrected by normalization to HPRT cDNA levels. Relative quantitation of target cDNA was determined by the formula $2^{-\Delta CT}$, with ΔCT denoting fold increases above WT.
For mitochondrial mass determination, genomic DNA from 1-2. 10^6 cells was extracted using the DNeasy Blood and Tissue Kit (Qiagen), following the manufacturer's instructions. DNA concentrations were determined by photometry (Gen5 BioTek) and 15 ng, 7.5 ng and 3.75 ng DNA were used to perform qPCR for mitochondrial gene *mtCOI* and nuclear gene *ndufv1*. Ratios of 2^{-CT} for *mtCOI* over *ndufv1* for the different DNA concentrations were averaged and fold of WT is shown.

Respiration and glycolysis
For real-time analysis of ECAR and OCR, IBMM were analyzed with a XF-24 Extracellular Flux Analyzer following the manufacturer's instructions (Seahorse Bioscience). Briefly, cells were seeded at 60,000 cells/well 24 h before the assay. For OCR measurements, 1 h before analysis, media was changed to XF base medium (Seahorse Bioscience) containing 25 mM glucose (Sigma), 2 mM L-glutamine and 1 mM sodium pyruvate (Invitrogen). Five consecutive measurements were obtained under basal conditions. Mitochondrial respiration was further characterized after the sequential addition of 1 µg/mL oligomycin A1 (Santa Cruz Biotechnologies), to inhibit mitochondrial ATP synthase; 3 µM FCCP (fluoro-carbonyl cyanide phenylhydrazone) (Santa Cruz Biotechnologies), a protonophore that uncouples ATP synthesis from oxygen consumption by the electron-transport chain, and 100 nM rotenone (Sigma-Aldrich), which inhibits the electron transport chain. Three consecutive measurements were made after each sequential treatment. Instrumental background was measured in separate control wells using the same conditions without biological material. Metabolic rates were normalized to cell numbers.
In this assay, basal oxygen consumption can be established by measurement of OCR in the absence of drugs. A decrease in OCR after the addition of oligomycin and rotenone is expected and indicates that cells are consuming oxygen for mitochondrial oxidative phosphorylation. In particular, the difference between basal OCR and after oligomycin treatment reveals OCR used for ATP production by the ATP synthetase. OCR at the end of the sequence corresponds to non-mitochondrial OCR. Proton leak, dependent on the proton gradient across the mitochondrial inner membrane, is the difference between non-mitochondrial OCR and OCR when the electron-transport chain is blocked by oligomycin. Maximal OCR occurs after the addition of FCCP, which dissipates the proton gradient, leading to oxygen reduction independently of ATP production. SRC is calculated as the difference between basal OCR and maximal OCR after the addition of FCCP.

Similarly, for glycolysis characteristics analysis, media was changed to XF base medium (Seahorse Bioscience) containing 2 mM L-glutamine (Invitrogen) 1 h prior analysis. ECAR was measured after the sequential addition of 10 mM glucose to induce glycolysis, 1 µg/mL oligomycin to force cells to increase glycolysis to the maximal rate (glycolytic capacity), and 100 mM glycolysis inhibitor 2-DG. Glycolytic reserve is the difference between glycolytic capacity and glycolysis.

Analysis of protein degradation pathways
10^6 IBMM cells (6 days after with tamoxifen treatment initiation) were plated in 6-cm dish and 24 h later, were incubated with 10 µM MG132 (Sigma) or 10 nM Bafilomycin A1 (Sigma) for 2, 6 and 24 h. Cells were washed twice with PBS, lysed in Triton lysis buffer (1 % Triton X-100, 150 mM NaCl, 50 mM HEPES pH 7.5, 5 mM EDTA) with 1 mM DTT and protease inhibitors (1 mM PMSF, 1 µg/mL aprotinin, 10 µg/mL pepstatin and 1 µg/mL leupeptin) and incubated for 20 min on ice. Lysates were then clarified at 15,000 rpm for 15 min at 4°C. Total cell lysates were fractionated by SDS-PAGE and analyzed by western blot.

Lentivirus generation and IBMM transduction

FUW-TetON vector was modified from FUW-TetON-hOCT4, a gift from Rudolf Jaenisch (Addgene plasmid # 20726, Hockemeyer, 2008), to include AgeI and NheI sites. NDUFAF1 cDNA was amplified from mouse macrophages total cDNA using forward primer 5' ataaccggtgccaccatggcaatgtcttccattcac 3' and reverse primer 5' atagctagcctatctgaagagtcttgggttaag and cloned into FUW-TetON between AgeI and NheI sites. For inducible expression upon Doxycyclin treatment, plasmid FUW-M2rtTA, a gift from Rudolf Jaenisch (Addgene plasmid # 20342, (Hockemeyer et al., 2008)), was used. Viral stocks were produced by calcium phosphate transfection of 293FT cells with FUW-TetON, FUW-TetON-NDUFAF1 or FUW-M2rtTA in combination with packaging vectors psPAX2, a gift from Didier Trono (Addgene plasmid # 12260), and envelope pCMV-VSV-G (Addgene plasmid #8454). Medium of 70 % confluent 293FT in 75 cm^2 flasks was changed 2 h before transfection. Calcium phosphate precipitates were prepared by mixing 12.5 µg FUW plasmid with 12.5 µg psPAX2 and 5 ug pCMV-VSV-G in water for a final volume of 875 uL. 125 uL 2 M $CaCl_2$ and 1 mL HBS 2X (50 mM HEPES, 10 mM KCl, 280mM NaCl, 1.5 mM Na_2HPO_4, pH 7.05) were sequentially added dropwise in slowly vortexed solution. Solutions were incubated at RT for 20 min and mixed gently to 293FT supernatant. Medium was replaced by 7 mL of culture medium 24 h later. Supernatants were collected, centrifuged at 1,500 rpm for 5 min and filtered. 500,000 IBMM were transduced with 1mL FUW-TetON or FUW-TetON-NDUFAF1 in conjunction with 0.5 mL FUW-M2rtTA lentiviral vectors, 6 ug/mL polybrene (Sigma) and 10 mM HEPES (Invitrogen) by spinfection at 1,800 rpm 27°C for 1h 30min in non-treated 12-well plate. 1mL fresh medium was added and spinfection was repeated the following day. iBMM were subsequently cultured in the presence of 10 % Tet System approved FBS (Takara #631107) instead of standard FBS. 48 h later, transduced iBMM were selected with 300 ug/ml zeocin (Invivogen) for 4 days and maintained in 100 ug/mL zeocin after selection.

5 days after tamoxifen treatment initiation, 250-500,000 transduced iBMM were plated in 6-well plates and after 24 hrs treated with 300 ng/mL doxycycline (Sigma) for 24 hrs, washed twice in PBS, lysed in Triton lysis buffer (1 % Triton X-100, 150 mM NaCl, 50 mM HEPES pH 7.5, 5 mM EDTA) with 1 mM DTT and protease inhibitors (1 mM PMSF, 1ug/mL aprotinin, 10ug/mL pepstatin and 1 ug/mL leupeptin), incubated 20 min on ice, clarified at 15,000 rpm for 15 min at 4°C, and supernatants collected. Total cell lysates were fractionated by SDS-PAGE and analyzed by western blotting.

ECSIT expression plasmids

To build ECSIT-3CFLAG plasmid, murine ECSIT2 was cloned from ECSIT-FLAG plasmid (West et al., 2011) into p3XFLAG-CMV14 (Sigma-Aldrich) between KpnI and XbaI sites using forward primer: 5'-ATAGGTACCGCCACCATGGGCAGCTGG-3' and reverse primer 5'-ATATCTAGAACTTTGCCCCTGCTGCTGC-3'. ΔMLS-3CFLAG was built similarly by cloning ECSIT2 amino acids 49 to 435 (without the mitochondrial localization sequence (MLS)) using forward primer: 5'-ATAGGTACCGCCACCATGGGCAAGGATG-3' and the same reverse primer as above.

Coimmunoprecipitation (coIP)

For ECSIT/PINK1 and ECSIT/LC3 coIPs, 1-2.10^6 293FT cells were plated in 6-cm dishes and transfected with 3 µL lipofectamine 2000 (Invitrogen) following the manufacturer's protocol. ECSIT/PINK1 coIP was performed using 0.25 µg ECSIT-3CFLAG, 1 µg pCMVTNT PINK1 C-myc (Beilina et al., 2005), 1 µg pMXs-IP HA-Parkin (Yoshii et al., 2011), and corresponding empty vector controls. For ECSIT/LC3 coIP, 0.5 µg ECSIT-3CFLAG, 2 µg YFP-LC3 (a king gift from the laboratory of T. Meila), and corresponding empty vector controls were used. The following day, cells were treated with 30 µM CCCP as indicated **(**carbonyl cyanide m-chlorophenyl hydrazine, Sigma-Aldrich). 24 h after transfection, cells were washed twice with PBS, lysed in 500 µL coIP buffer (150 mM NaCl, 25 mM Hepes, 0.2% NP40, 10% Glycerol) with 1 mM DTT and protease inhibitors (1 mM PMSF, 1 µg/mL aprotinin, 10 µg/mL pepstatin and 1 µg/mL leupeptin), incubated for 20 min on ice and, clarified at 15,000 rpm for 15 min at 4°C. A sample was aliquoted for input and remaining lysate was incubated for 6 h at 4°C with 0.5 µg anti-FLAG antibody (Sigma-Aldrich, clone M2) or anti-Myc-Tag antibody (Cell Signaling, clone 9B11) and overnight with 10 µL of washed Protein G sepharose 4B beads (Invitrogen). Beads were washed in coIP buffer and resuspended in 2X Laemmli buffer. Samples were fractionated by SDS-PAGE and analyzed by western blotting.

Ubiquitination Assay

2.10^6 293FT cells were plated in 6-cm dishes and transfected with 3 µL lipofectamine 2000 (Invitrogen) and 0.25 µg ECSIT-3CFLAG, 0.1 µg ΔMLS-3CFLAG, 1 µg pCMVTNT PINK1 C-myc (Beilina et al., 2005), 1 µg pMXs-IP HA-Parkin (Yoshii et al., 2011), 1 µg pcDNA3 VSV-Ubiquitin (Chastagner et al.) and corresponding empty vector controls, following the manufacturer's protocol. 24 h after transfection, cells were washed twice with PBS,

solubilized in 200 µL boiling SDS lysis buffer (20 mM Tris-HCl, 1% SDS, pH 7.5) and boiled for an additional 10 min. After shearing DNA, the samples were diluted to 0.4 % SDS with water, then an equal volume of 2X TNT buffer (50 mM Tris-HCl pH 7.4, 300 mM NaCl, 2% Triton X-100, 20% glycerol, 2 mM EDTA, 2X protease inhibitors) was added. An aliquot was taken for input and remaining samples were immunoprecipitated with 1 µg anti-VSV-G antibody (Sigma-Aldrich, clone P5D4) for 6 h at 4°C and overnight with 10 µL of washed Protein G sepharose 4B beads (Invitrogen). Beads were washed in TBS (50mM Tris HCl pH7.4, 150mM NaCl) and resuspended in 2X Laemmli buffer. Samples were fractionated by SDS-PAGE and analyzed by western blotting.

Analysis of mitochondrial damage induction in macrophages

WT IBMM and BMDM were plated in 10 cm tissue culture dish (3.10^6 cells/well) and, the following day, treated with 100 ng/mL LPS, 10 µM CCCP and 10 nM Bafilomycin A1 or DMSO control (Sigma-Aldrich) for 1h. Cells were lysed in coimmunoprecipitation buffer and processed as described above using anti-mouse ECSIT2 antibody (West et al). For time course of treatment, cells were treated with 100 ng/mL LPS, 30 µM CCCP or DMSO control for 15, 30 and 60 min, washed twice in PBS, lysed in 1% SDS lysis buffer as above (Ubiquitination assays).
For coimmunoprecipitation, cells were treated with 10 nM Bafilomycin A1 (Ba1) for 5h and/or 20 µM of CCCP (CC) for 1h. Cells were washed twice with PBS, lysed in 500 µL coIP buffer (150 mM NaCl, 25 mM Hepes, 0.2% NP40, 10% Glycerol) with 1 mM DTT and protease inhibitors (1 mM PMSF, 1 µg/mL aprotinin, 10 µg/mL pepstatin and 1 µg/mL leupeptin), incubated for 20 min on ice and, clarified at 15,000 rpm for 15 min at 4°C. A sample was aliquoted for input and remaining lysate was incubated for 6 h at 4°C with anti-ECSIT2 antibody (West et al, 2011) or IgG control (Cell Signaling, #2729) and overnight with 30 µL of washed Protein G sepharose 4B beads (Invitrogen). Beads were washed in coIP buffer and resuspended in 2X Laemmli buffer. Samples were fractionated by SDS-PAGE and analyzed by western blotting.

SDS-PAGE and Western blotting

Protein concentrations were determined using the microBCA protein kit (Thermo Scientific). 20-40 µg total cell lysate or 10-20 µg solubilized mitochondrial proteins from BMDM or IBMM were separated by SDS-PAGE and transferred onto a PVDF membrane (Immobilon-P, Millipore).
Membranes for SDS-PAGE and Blue Native PAGE were blocked in 5 % non-fat milk and incubated with primary and horseradish peroxidase (HRP)–conjugated secondary antibodies. We used Super Signal West Pico chemiluminescent substrate (Thermo Fisher Scientific) or Luminata Forte (Millipore) and BioExcell autoradiographic films (WWMP) for image development. Primary antibodies were: anti-VDAC1 (Abcam, clone 20B12AF2), ubiquitin (Santa Cruz, clone P4D1), NDUFS3 (Abcam, clone 3F9DD2), ND6 (Molecular Probe, clone 20E9), SDHA (Abcam, clone EPR9043), UQCRC2 (Abcam, clone 13G12AF12BB11), ATP synthase F1 alpha and beta subunits (kindly provided by Dr. *Alexander Tzagoloff*, Columbia University), NDUFAF1 (Origene), TOM20 (Sigma, clone 4F3), GAPDH (Fitzgerald), beta-Tubulin (Sigma, clone TUB2.1), HDAC1 (Santa Cruz), Parkin (Cell Signaling, Prk8), PINK1 (Novus Biologicals), LC3b (Sigma-Aldrich), Myc (Cell Signaling, clone 9B11), HA (Sigma-Aldrich, clone HA-7), FLAG (Sigma-Aldrich, clone M2), and ECSIT (rabbit polyclonal antibody against ECSIT was previously described (West et al, 2011)).

Quantification and Statistical Analysis

Statistical analysis was conducted using GraphPad Prism 6 software. All data were tested for normal distribution of variables. All normally distributed data were displayed as means ± standard deviation (SD) unless otherwise noted. Measurements between two groups were performed with an unpaired Student's t test if normally distributed, or Mann-Whitney U test if otherwise. Groups of three or more were analyzed by one-way analysis of variance (ANOVA) or the Kruskal-Wallis test. Values of n for each experiment are reported in the figures and figure legends. $p < 0.05$ was considered significant. Statistical parameters for each experiment can be found within the corresponding figure legends.

Primer name	Sequence (5'-3')
LNeoL_intron3F	CTGCCAGATTAGCTCATGGTACTTCATCACAGTAACAGGGAAGCACTAGTACAGAAGTTGCCGATCATATTCAATAACCCTTAAT
LNeoL_intron3R	ACACACGCATACACACACGCGAAGAAAACATCAAGAAGCATTGCCAGGACCACATTGTTGCTAGTGGATCCCCTCGAGGGACCTA
FNeoFL_intron4F	GTTGCTGGGATTTGAACTTTGGACCTTCTGAAGAACAGTCGGGTGCTCTTACCCACTGAGATCGATAAGCTTGATATCGAATTCC
FNeoFL_intron4R	GTACCTATCTCCAGACACACAAGAATAGGACATCAGATCCCATTATGGATGGTTGTGAACGCTCTAGAACTAGTGGATCCACCTA
Ret_Left1_ECSIT	CTGAGTTTAAGGCCAGCTTGGTCTACACAGCAACTTCCAGATTAGCCGGCGCGCCAGTGTGGTTTTCAAGAGGA
Ret_Right1_ECSIT	CCCATTGCGAGAGAATTTTATAGTCATATTCAAGAGGCACTAGTGTGCAGCGGCCGCAATTCGCCCTATAGTGAGT
longarm2F	CATGTTCTCTGTGGCCTAGATAC
L83 loxp	CCTCGAGGGACCTAATAACTTCGTA
Short_arm1R	GCCAGGCGGAATACCACTGG
ARM2/F2	CGTTGGCTACCCGTGATATT

List of primers used for qPCR

Gene	Forward primer (5'-3')	Reverse primer (5'-3')
Hprt	GTTAAGCAGTACAGCCCCAAA	AGGGCATATCCAACAACAAACTT
HIF1a	GGGGAGGACGATGAACATCAA	GGGTGGTTTCTTGTACCCACA
GLUT1	AGCCCTGCTACAGTGTAT	AGGTCTCGGGTCACATC
PKM2	GCCGCCTGGACATTGACTC	CCATGAGAGAAATTCAGCCGAG
PFKFB1	ATGAGCTGCCCTATCTCAAGT	GTCCCGGTGTGTGTTCACAG
PFKFB3	CAACTCCCCAACCGTGATTGT	GAGGTAGCGAGTCAGCTTCTT
LDHA	AGGCTCCCCAGAACAAGATT	TCTCGCCCTTGAGTTTGTCT
MCT1	TGTTAGTCGGAGCCTTCATTTC	CACTGGTCGTTGCACTGAATA
bTub	CCCTCAGCTTTCTCCAACTG	CACCATTTACCCCCAATGAG
mtND6	GGTTAGCATTAAAGCCTTCACCT	CATCAACCAATCTCCCAAACCAT
NDUFS3	TGGCAGCACGTAAGAAGGG	CTTGGGTAAGATTTCAGCCACAT
NDUFAF1	TGTCCTTGTAAGCCCTCTTCAG	TTTGTGGGTAGTCACTGTGTAGA
Uqcrc2	AAAGTTGCCCCGAAGGTTAAA	GAGCATAGTTTTCCAGAGAAGCA
SDHA	GGAACACTCCAAAAACAGACCT	CCACCACTGGGTATTGAGTAGAA

ATP5a1	TCTCCATGCCTCTAACACTCG	CCAGGTCAACAGACGTGTCAG
mtCOI	TGCTAGCCGCAGGCATTAC	GGGTGCCCAAAGAATCAGAAC
Ndufv1	CTTCCCCACTGGCCTCAAG	CCAAAACCCAGTGATCCAGC

Other Resources Table

REAGENT or RESOURCE	SOURCE	IDENTIFIER
Antibodies		
Anti-mouse ECSIT2, rabbit polyclonal	(Kopp et al., 1999)	N/A
Anti-VDAC1, mouse monoclonal (20B12AF2)	Abcam	Cat#ab14734, RRID:AB_443084
Anti-ubiquitin, mouse monoclonal (P4D1)	Santa Cruz Biotechnology	Cat#sc-8017, RRID:AB_628423
Anti-NDUFS3, mouse monoclonal (3F9DD2)	Abcam	Cat#ab110246, RRID:AB_10861972
Anti-ND6, mouse monoclonal (20E9)	Dr Malgorzata Rak/ Thermo Fischer	Cat#A31857, RRID:AB_1501823
Anti-SDHA, rabbit monoclonal (EPR9043)	Abcam	Cat#ab137040
Anti-Uqcrc2, mouse monoclonal (13G12AF12BB11)	Abcam	Cat#ab14745, RRID:AB_2213640
Anti-ATP synthase F1 alpha subunit, rabbit polyclonal	Dr. Alexander Tzagoloff, Columbia University	(Rak et al., 2011)
Anti-ATP synthase F1 beta subunit, rabbit polyclonal	Dr. Alexander Tzagoloff, Columbia University	(Rak et al., 2011)
Anti-NDUFAF1, rabbit polyclonal	OriGene	Cat#TA30792
Anti-TOM20, mouse monoclonal (4F3)	Sigma-Aldrich	Cat#WH0009804M1, RRID:AB_1843992
Anti-LC3b, rabbit polyclonal	Sigma-Aldrich	Cat#L7543, RRID: AB_796155
Anti-Parkin, mouse monoclonal	Cell Signaling	Cat#4211S, RRID:AB_10694914
Anti-PINK1, rabbit polyclonal	Novus Biologicals	Cat#BC100-494, RRID:AB_10127658
Anti-HDAC1, rabbit polyclonal	Santa Cruz Biotechnology	Cat#sc7872, RRID:AB_2279709
Anti-GAPDH, mouse monoclonal (6C5)	Fitzgerald	Cat#10R-G109a, RRID:AB_1285808
Anti-beta-Tubulin, mouse monoclonal (TUB2.1)	Sigma-Aldrich	Cat#T4026, RRID:AB_477577
Anti-FLAG, mouse monoclonal (M2)	Sigma-Aldrich	Cat#F1804, RRID:AB_262044
Anti-VSV-G, mouse monoclonal (P5D4)	Sigma-Aldrich	Cat#V5507, RRID:AB_261877
Anti-Myc-Tag, mouse monoclonal (9B11)	Cell Signaling	Cat#2276S, RRID:AB_331783
Anti-HA, mouse monoclonal (HA-7)	Sigma-Aldrich	Cat#9658, RRID:AB_260092

Anti-CD16/CD32 (2.4G2)	Tonbo Biosciences	Cat#70-0161, RRID:AB_2621487
Anti-F4/80-FITC (BM8)	eBiosciences	Cat#11-4801-81, RRID:AB_465226
CD11b-PE (M1/70)	eBiosciences	Cat#12-0112-81, RRID:AB_465546
Ly6G-VF405	Tonbo Biosciences	Cat#75-1276, RRID:AB_2621955
CD3-PerCPCy5.5 (145-2C11)	Tonbo Biosciences	Cat#65-0031, RRID:AB_2621872
B220-APC780 (RA3-6B2)	eBiosciences	Cat#47-0452-82, RRID:AB_1518810
Bacterial and Virus Strains		
E. coli SW106	Liu et al., 2003	(Liu et al., 2003)
Chemicals, Peptides, and Recombinant Proteins		
4OH-Tamoxifen	Sigma-Aldrich	Cat#H6278, CAS 68392-35-8
DDM (Dodecylmaltoside)	Sigma-Aldrich	Cat#D4641, CAS 69227-93-6
Aminohexanoic acid	Sigma-Aldrich	Cat#07260, CAS 60-32-2
Coomassie Blue G-250	AmericanBIO	Cat#AB00325, CAS 6104-58-1
Sodium Pyruvate	Thermo Fisher	Cat#11360070
L-Glutamine	Thermo Fisher	Cat#25030081
MitoSOX Red Mitochondrial Superoxide Indicator	Thermo Fisher	Cat#M36008
Tetramethylrhodamine, Methyl Ester, Perchlorate (TMRM)	Thermo Fisher	Cat#T668
Mitotracker Green FM	Thermo Fisher	Cat#M7514
CM-H_2DCFDA chloromethyl derivative of 2',7'-dichlorodihydrofluorescein diacetate	Thermo Fisher	Cat#C6827
Imperial Protein Stain	Thermo Fisher	Cat#24615
Nitro blue tetrazolium (NBT)	Research Products International	Cat#66000-0.1, CAS 298-83-9
Chloramphenicol	Sigma-Aldrich	Cat#C0378, CAS 56-75-7
2-Deoxyglucose (2-DG)	Sigma-Aldrich	Cat#D6134, CAS 154-17-6
D-(+)-Glucose	Sigma-Aldrich	Cat#G8270, CAS 50-99-7
D-(+)-Galactose	Sigma-Aldrich	Cat#G0625, CAS 59-23-4
Sodium oxamate	Sigma-Aldrich	Cat#O2751, CAS 565-73-1
LPS from E. *coli* 026:B6	Sigma-Aldrich	Cat#8274
Recombinant mouse M-CSF	R&D Systems	Cat#416-ML
Oligomycin	Santa Cruz Biotechnology	Cat#sc-203342, CAS 1404-19-9

FCCP	Santa Cruz Biotechnology	Cat# sc-203578, CAS 370-86-5
Rotenone	Sigma-Aldrich	Cat#8875, CAS 83-79-4
Antimycin	Sigma-Aldrich	Cat#A8674, CAS 1397-94-0
MG132	Calbiochem/Millipore	Cat#474790, CAS 133407-82-6
Bafilomycin A1	Sigma-Aldrich	Cat#B1793, CAS 88899-55-2
Zeocin	Invivogen	Cat#ant-zn-1, CAS 11006-33-0
CCCP	Sigma-Aldrich	Cat#2759, CAS 555-60-2
Doxycyclin	Sigma-Aldrich	Cat#3447, CAS 10592-13-9
Dnase I	Sigma-Aldrich	Cat#D4513, CAS 9003-98-9
Collagenase	Sigma-Aldrich	Cat#C5138, CAS 9001-12-1
Critical Commercial Assays		
L-lactate assay Kit I	Eton Bioscience	Cat#120001100P
Complex I Enzyme Activity Assay Kit	Abcam	Cat# ab109721
NAD/NADH Quantitation Colorimetric Kit	BioVision	Cat#K337
ATPlite Luminescence Assay System	Perkin Elmer	Cat#6016943
RNeasy Mini Kit	QIAGEN	Cat#74104
DNeasy Blood and Tissue Kit	QIAGEN	Cat#69504
PerfeCTa SYBR Green FastMix	QantaBio	Cat#95072
Seahorse FluxPak Mini	Seahorse Bioscience/Agilent	Cat#100867-100
Seahorse XF Base medium	Seahorse Bioscience/Agilent	Cat#102353100
Mouse IL-6 ELISA Set	BD Biosciences	Cat#555240
Mouse TNF (Mono/Mono) ELISA Set	BD Biosciences	Cat#555268
Experimental Models: Cell Lines		
Mouse: L929	ATCC	CCL-1
Human: 293FT	ThermoScientific	R70007
Mouse: ψCREJ2	Laboratory of KA Fitzgerald	(Hornung et al., 2008)
Mouse: iBMM ECSIT$^{f/f}$/Cre-ERT2^{+}	This paper	N/A
Experimental Models: Organisms/Strains		
Mouse: ECSIT CKO : ECSIT$^{f/f}$	This paper	N/A
Mouse: ECSIT KO : ECSIT$^{+/-}$	(Xiao et al., 2003)	(Xiao et al., 2003)
Mouse: LysM-Cre : B6.129P2-*Lyz2*$^{tm1(cre)Ifo}$/J	The Jackson Laboratory	Stock 004781
Mouse: Cre-ERT2 : Rosa26Cre-ERT2	Laboratory of B. Reizis (Thomas Ludwig)	Unpublished
Mouse : C57BL/6	The Jackson Laboratory	Stock 000664

Oligonucleotides		
Primers for *Escit* conditional knockout mouse generation, See Table S1	This paper	N/A
Primers for qPCR, See Table S2	This paper	N/A
Primer NDUFAF1 cloning forward: ataaccggtgccaccatggcaatgtcttccattcac	This paper	N/A
Primer NDUFAF1 cloning reverse: atagctagcctatctgaagagtcttgggttaag	This paper	N/A
Primer ECSIT-3CFLAG cloning forward: ataggtaccgccaccatgggcagctgg	This paper	N/A
Primer ECSIT-3CFLAG cloning reverse: atatctagaactttgcccctgctgctgc	This paper	N/A
Primer ΔMLS-3CFLAG cloning forward: ataggtaccgccaccatgggcaaggatg	This paper	N/A
Recombinant DNA		
pL452	Frederick National Laboratory NCI	(Liu et al., 2003)
pL451	Frederick National Laboratory NCI	(Liu et al., 2003)
pMCS-DTA	Kosuke Yusa, Wellcome Trust Sanger Institute	(Yusa et al., 2011)
FUW-TetON-hOCT4	(Hockemeyer et al., 2008)	Addgene #20726
FUW-TetON	This paper	N/A
FUW-M2rtTA	(Hockemeyer et al., 2008)	Addgene #20342
FUW-TetON-NDUFAF1	This paper	N/A
psPAX2	Laboratory of D. Trono	Addgene #12260
pCMV-VSV-G	(Stewart et al., 2003)	Addgene #8454
ECSIT-FLAG	(West et al., 2011)	N/A
p3XFLAG-CMV14	Sigma-Aldrich	Cat#E7908
pCMVTNT PINK1 C-myc	(Beilina et al., 2005)	Addgene # 13314
pMXs-IP HA-Parkin	(Yoshii et al., 2011)	Addgene # 38248
pcDNA3 VSV-G Ubiquitin	(Chastagner et al., 2006)	N/A
YFP-LC3	Laboratory of T. Meila	N/A
Software and Algorithms		
GraphPad Prism 6	GraphPad	https://www.graphpad.com/scientific-software/prism/
FlowJo	FlowJo, LLC	https://www.flowjo.com/solutions/flowjo
Other		
Tet System approved FBS	Takara	Cat#631107
DMEM, no glucose	Thermo Fisher	Cat#11966025
DMEM, no glucose, no glutamine	Thermo Fisher	Cat#A1443001
NativePAGE 4-16 % Bis-Tris Protein gel	Thermo Fisher	Cat#BN1002BOX

Supplemental References

Beilina, A., Van Der Brug, M., Ahmad, R., Kesavapany, S., Miller, D.W., Petsko, G.A., and Cookson, M.R. (2005). Mutations in PTEN-induced putative kinase 1 associated with recessive parkinsonism have differential effects on protein stability. Proc Natl Acad Sci U S A *102*, 5703-5708.

Blasi, E., Radzioch, D., Durum, S.K., and Varesio, L. (1987). A murine macrophage cell line, immortalized by v-raf and v-myc oncogenes, exhibits normal macrophage functions. Eur J Immunol *17*, 1491-1498.

Blasi, E., Radzioch, D., Merletti, L., and Varesio, L. (1989). Generation of macrophage cell line from fresh bone marrow cells with a myc/raf recombinant retrovirus. Cancer Biochem Biophys *10*, 303-317.

Chastagner, P., Israel, A., and Brou, C. (2006). Itch/AIP4 mediates Deltex degradation through the formation of K29-linked polyubiquitin chains. EMBO Rep *7*, 1147-1153.

Diaz, F., Barrientos, A., and Fontanesi, F. (2009). Evaluation of the mitochondrial respiratory chain and oxidative phosphorylation system using blue native gel electrophoresis. Current protocols in human genetics *Chapter 19*, Unit19 14.

Hockemeyer, D., Soldner, F., Cook, E.G., Gao, Q., Mitalipova, M., and Jaenisch, R. (2008). A drug-inducible system for direct reprogramming of human somatic cells to pluripotency. Cell stem cell *3*, 346-353.

Kopp, E., Medzhitov, R., Carothers, J., Xiao, C., Douglas, I., Janeway, C.A., and Ghosh, S. (1999). ECSIT is an evolutionarily conserved intermediate in the Toll/IL-1 signal transduction pathway. Genes & development *13*, 2059-2071.

Liu, P., Jenkins, N.A., and Copeland, N.G. (2003). A highly efficient recombineering-based method for generating conditional knockout mutations. Genome research *13*, 476-484.

Nijtmans, L.G., Henderson, N.S., and Holt, I.J. (2002). Blue Native electrophoresis to study mitochondrial and other protein complexes. Methods *26*, 327-334.

Palleroni, A.V., Varesio, L., Wright, R.B., and Brunda, M.J. (1991). Tumoricidal alveolar macrophage and tumor infiltrating macrophage cell lines. Int J Cancer *49*, 296-302.

Rao, P., Hayden, M.S., Long, M., Scott, M.L., West, A.P., Zhang, D., Oeckinghaus, A., Lynch, C., Hoffmann, A., Baltimore, D.*, et al.* (2010). IkappaBbeta acts to inhibit and activate gene expression during the inflammatory response. Nature *466*, 1115-1119.

West, A.P., Brodsky, I.E., Rahner, C., Woo, D.K., Erdjument-Bromage, H., Tempst, P., Walsh, M.C., Choi, Y., Shadel, G.S., and Ghosh, S. (2011). TLR signalling augments macrophage bactericidal activity through mitochondrial ROS. Nature *472*, 476-480.

Wittig, I., Braun, H.P., and Schagger, H. (2006). Blue native PAGE. Nature protocols *1*, 418-428.

Xiao, C., Shim, J.H., Kluppel, M., Zhang, S.S., Dong, C., Flavell, R.A., Fu, X.Y., Wrana, J.L., Hogan, B.L., and Ghosh, S. (2003). Ecsit is required for Bmp signaling and mesoderm formation during mouse embryogenesis. Genes & development *17*, 2933-2949.

Xiao, C., Wang, R.H., Lahusen, T.J., Park, O., Bertola, A., Maruyama, T., Reynolds, D., Chen, Q., Xu, X., Young, H.A.*, et al.* (2012). Progression of chronic liver inflammation and fibrosis driven by activation of c-JUN signaling in Sirt6 mutant mice. J Biol Chem *287*, 41903-41913.

Yoshii, S.R., Kishi, C., Ishihara, N., and Mizushima, N. (2011). Parkin mediates proteasome-dependent protein degradation and rupture of the outer mitochondrial membrane. J Biol Chem *286*, 19630-19640.

Yusa, K., Rashid, S.T., Strick-Marchand, H., Varela, I., Liu, P.Q., Paschon, D.E., Miranda, E., Ordonez, A., Hannan, N.R., Rouhani, F.J.*, et al.* (2011). Targeted gene correction of alpha1-antitrypsin deficiency in induced pluripotent stem cells. Nature *478*, 391-394.